BROWNIAN DYNAMICS SIMULATIONS OF DILUTE POLYMER SOLUTIONS WITH ENTANGLEMENTS

by

Sean Patrick Holleran

A dissertation submitted in partial fulfillment
of the requirements for the degree of
Doctor of Philosophy
(Chemical Engineering)
in The University of Michigan
2007

Doctoral Committee:

Professor Ronald G. Larson, Chair
Professor Sharon C. Glotzer
Associate Professor Michael J. Solomon
Associate Professor Michael Falk

To my mom …

who has waited seven years to call me “Dr. Holleran”

ACKNOWLEDGEMENTS

I wish to begin by thanking my thesis advisor Professor Ron Larson. This has been a long and challenging process, and I have by no means followed a traditional path, but Ron has been a consistent and positive force moving me toward my graduation. I appreciate his guidance and focus in my research and his patience and understanding in my various extra curricular organizations, activities, and involvements. I am happy to say that I have had a very good relationship with my advisor.

I wish to also thank the members of my doctoral committee – Professor Sharon Glotzer, Associate Professor Michael Solomon, and Associate Professor Michael Falk. Their advice and comments on the direction of my research has helped me develop a thorough and complete dissertation. I also want to thank Professor Robert Ziff for attending my oral defense on short notice.

I have had the pleasure of teaching with many of the faculty in the chemical engineering department – I am grateful for the opportunity to work alongside such a large number of educators. Dr. Robert Lionberger, Professor Sharon Glotzer, Professor James Wilkes, Professor Phil Savage, Professor Mark Burns, Professor Johannes Schwank, Assistant Professor Nina Lin, and Mr. Barry Barkel have all been colleagues of mine in an

undergraduate classroom. I have especially enjoyed the countless conversations I have shared with Barry while teaching senior design for the past two years.

Many of my fellow chemical engineering graduate students have worked with me in teaching a variety of courses. I am pleased to thank Stacy Pyett, Tesfu Solomon, Elaine Chan, Worojit Setthapun, Fang Wang, Ben Gould, and Tom Gilbert for numerous problem sets, discussions, lecture notes, re-grades, office hours, review sessions, recitation preparations, and shoulders to lean on.

Other fellow graduate students have been helpful to my research. Chris Iacovella provided me with the ability to generate small movies that do wonders to illustrate the outcomes of my work. Senthil Kandasamy has shared one office and many enlightening conversations (not all about my research) with me for the past three years. Former Larson group members Lei Li and Chih Chen Hsieh each provided me with some of their own previous work that I used to build my research upon. Other members of the Larson group (past and present) who deserve recognition include Hua Hu, Anshuman Roy, Manish Chopra, Ji Hoon Kim, Bruce Shiamberg, and Sachin Shanbhag.

I must thank Dr. Susan Montgomery for her endless assistance and never-ending best wishes. Susan was beyond valuable to my professional development. I worked closely with her in her role as the faculty advisor to the American Society for Engineering Education, as a student in her Teaching Engineering course, and as fellow proponent of

excellence in undergraduate education. I will forever appreciate her guidance and advice during my job search.

I am grateful to Ben Gould and Greg DiLeo (the *lunch bunch*) for being my best friends here at Michigan. I will remember how we always found the time for off-campus burrito lunches and bear poker that one summer. I also want to thank my former roommate (and fourth member of the *not-from-Michigan* poker club) Mike Geiger. Those were a lot of early mornings at the gym / late evenings watching cartoons / Sunday nights at Ashley's (the first year) that we spent together. Other chemical engineering friends of mine (many whom have already graduated) that I would like to acknowledge are Elaine Chan, Chris Brinkerhoff, Stephanie Teich-McGoldrick, Andre Taylor, Eric Jankowski, Craig Comisar, and Andrew Tadd. I also wish to thank the friends of mine who love snacks – they know who they are – it has been fun.

I thank Lisa Briand for being beside me for nearly two years. I am grateful that we have been together as I have finished the final stages of this work – and I look forward to being together as we each move ahead to the next stages of our lives. Thank you Lisa – you helped make this happen.

Most importantly – I thank my family for making me what I am today. I thank my brother and sister for a healthy balance between sibling rivalries, conspiring against our parents, and being there for advice. I thank my mom and dad for building a home that encourages education, for attending every glee club concert / football game / high school

musical / piano recital they could make it to, for embarrassing me with their pride in front of friends and relatives, for being there for me whenever I needed them, and for always believing that I could accomplish anything. I hope that I will continue to make them proud.

TABLE OF CONTENTS

LIST OF FIGURES

Chapter 1

Chapter 2

Chapter 3

ABSTRACT

This dissertation describes the development of a bead-spring Brownian dynamics model for simulating the topological interactions between polymers and thin obstacles. We apply this method to electrophoretically translating DNA strands interacting with an immovable post. The use of a bead-spring method allows for the simulation of entanglement interactions of polymer chains too long to be simulated using bead-rod or pearl necklace models. This new method determines the shortest distance between a spring and the post, calculates a repulsive force inversely related to this distance using an exponential potential, and corrects for the rare situation when a spring passes beyond the post despite the repulsive interaction.

We consider single-chain collisions with a single post in weak electric fields. We explore a wide range of chain lengths ($25 \le N_K \le 1500$) and field strengths ($10^{-4} \le Pe_{Kuhn} \le 10^{0}$), and we find that the average delay produced by the collision is a function of both the chain length and the Peclet number. Our results are consistent with published results for a 25 Kuhn-step chain at Peclet number $Pe_{Kuhn} = 1.0$. Our new method is a general one that allows us to compute the effects of entanglements in systems with rare entanglements and long chains that cannot be simulated by other more microscopic methods.

We find that the mean distance $\langle \Delta \bar{x} \rangle$ that the chain migration is held up by the entanglement interaction increases with higher fields and encompasses four distinct regimes. The two fastest regimes exhibit the classic rope-and-pulley dynamics, in which the chain is draped around the entanglement and the longer of the two dangling ends pulls the shorter end around the obstacle. In the highest field strength regime, the dimensionless delay distance reaches its theoretical upper limit at $\langle \Delta \bar{x} \rangle / N_K = 0.5$. In the moderately high field strength regime, the ends of the chain remain balled up while the central portion is extended, creating a "ball and chain" configuration. In the two slower regimes, the polymer retains a coil-like shape as it diffuses laterally and eventually clears the post without deforming. We develop models that describe both the average delay and the distribution of delays for the three highest field regimes.

CHAPTER 1

INTRODUCTION

1.1 CAPILLARY ELECTROPHORESIS

Capillary electrophoresis is a process that has multiple applications. It is widely used for the separation of polymer molecules based on their molecular size. It is a successful procedure for quick and efficient separation of DNA segments.[1] This technology has experienced rapid development in recent years, and it is utilized for the separation of biopolymers, polysaccharides, and proteins. Medical diagnostics, drug development, forensics, and gene therapy all make use of capillary electrophoresis.[2]

The process takes place in a small capillary tube. Polyelectrolyte molecules translate through the tube under the influence of an electric field. The strength of the field, namely the voltage difference between the ends of the tube, divided by the length of the tube, is one variable that controls how rapidly the polymers migrate along the distance. If the capillary tube is filled only with solvent, the advancing polyelectrolyte behavior will be of the free-draining limit. Size dependent separation will not be achieved. Larger chains' forward motion is retarded by their increased frictional drag, but their forward motion is also more greatly enhanced by the electric field. Both of these effects scale linearly with the size of the polymer. A longer chain, relative to a smaller chain, will have difficulty

advancing because of its weight, but it will be further driven by the electric potential, and no relative difference in rates of migration between long and short chains will be achieved.

Some type of obstacle in the path of the polyelectrolyte is required to achieve the size dependent separation that is sought. It is thus necessary to introduce a second level of flow retardation that will be a function of the chain length. Sieving matrices are commonly established to impart a frictional drag on the DNA molecule proportional to its length.[2] Electrophoretic separations are thus nearly always performed in the presence of a neutral support matrix.[3]

1.1.1 Dense Solution

The traditional procedure has been to use a gel or a network of cross-linked polymer as the sieving medium. The gel is believed to act as a molecular sieve discriminating based on molecular size.[4] This dense mesh severely hinders the motion of all size DNA progressing forward; however, it more heavily slows the longer chains as they have a higher probability of interacting with the mesh.

Two theories exist to explain how a DNA molecule travels through this sieving matrix. The DNA in the absence of the imposed obstacle will be in a coiled conformation. This is the most entropically favored conformation. When the radius of gyration of the DNA coil is smaller than the average pore size in the mesh, the separation process is believed

to occur by Ogston sieving. If the radius of gyration is greater than the average pore size in the mesh, the process is believed to occur by reptation. Both of these processes result in making the mobility of a polymer chain a function of molecular size.

The Ogston theory[5] proposes that the DNA molecules move through the capillary tube maintaining their spherical shape. As they attempt to penetrate the mesh they must move about until they find a pore size large enough to fit through. This is sufficient to result in size dependent separation. A longer strand of DNA will form a coiled sphere with a greater radius of gyration than that of a shorter strand, and a sphere with a greater radius of gyration will have a more challenging and time-consuming process of finding a pore though which to advance. Longer strands of DNA will therefore take more time to translate the length of the capillary. The Ogston theory claims that DNA coils having a radius of gyration greater than the average pore size will not be able to move through the tube. Experiments have shown this to be false. A second theory is needed to explain this phenomenon.

The reptation theory proposes that the DNA molecules can leave their spherical shape to allow themselves to move through the open pores. The polymer can stretch and shrink along its own backbone while confined to a tube defined by the neighboring presence of the sieving matrix on its sides. A DNA molecule with a radius of gyration too large to fit through a pore may change its shape to achieve diffusion. Again, this is enough to result in size-dependent separation. A longer strand of DNA will have a more difficult and time-consuming process of rearranging its form by reptation. As with the Ogston model,

longer strands of DNA will therefore take more time to translate the length of the capillary.

1.1.2 Dilute Solution

Recent work has found that size-dependent separation in capillary electrophoresis is not wholly dependent on the presence of a gel or a dense cross-linked network.[6,7,8] Solutions of un-cross-linked polymers over a wide range of concentrations have been found to have potential to separate DNA molecules.[1] It has been shown that good separations are possible in un-cross-linked polymer solutions in dilute solutions near or at least an order of magnitude below the minimum entanglement concentration.[9,10] New attention has therefore concentrated on applications of electrophoresis that replace the traditional gel media with a dilute neutral polymer solution.[11] Hyrdoxyethyl cellulose (HEC) has been used as the obstacle in dilute solution. It works well because it is inflexible and therefore highly extended in solution. Size-dependent separation is still observed even though the process no longer involves entanglement with an extended matrix, but instead that of a DNA strand encountering sequentially a series of isolated polymer molecules.

There are a number of considerable advantages to performing capillary electrophoresis in dilute solution rather than in a dense gel network. Gels are unfavorable because their short capillary lifetimes, loss of reproducibility over time, and difficulty of introducing the matrix into the capillary tube. Dilute polymer solutions are more versatile and easier

to use.[2] The same level of separation requires more time in a gel because the DNA must move through the solution. For any given tube length and field strength, separations have been found to be five to ten times faster in dilute polymer solutions than is possible in conventional entangled polymer network solutions.[12] The dilute approach is also easier to consider from the viewpoint of computer simulations. Modeling the behavior of a small number of neutral polymer stands is far less expensive than building an entire network of polymers. The computationally intensive calculations are those surrounding the moments of interaction between the charged DNA and the neutral polymer. The percentage of time occupied by these interactions in the dilute situation is significantly lower in dilute solutions than in the dense situation. The advantage gained is that more time is spent performing relatively faster calculations.

The discovery that dilute systems of polymers can be used for capillary electrophoresis allows for a more complete capitalization on the speed and efficiency of the capillary geometry. The molecular dynamics explaining the interactions between charged DNA and neutral polymers, and how they may be different from those in the gel media, are not fully understood. Comprehending this mechanism is important for developing procedures to optimize the effectiveness of electrophoresis. Some groups believe that the mechanism is virtually identical to that in traditional slab gel electrophoresis[6], while others ascribe separation to the attraction and interaction of DNA with the cellulose strand in the buffer.[8] Beebe-Poli[13] performed capillary electrophoresis in un-cross-linked HEC by separating different lengths of polystyrene. They concluded after analysis of their data that neither Ogston sieving nor reptation were adequate mechanisms to

model their results. Viovy[14] and Duke[15] argue that separations are permissible in dilute solutions because the individual polymer strands act as the obstacles through which the DNA must travel. Barron[1] proposes that individual DNA chains become entangled with the discrete polymer molecules and they pull them along through the solution. Separation is achieved because the likelihood of entanglement between DNA and polymer increases with the size of the DNA chain. Hubert[16] also believes in a mechanism in which the host polymer is dragged forward a distance by the translating polyelectrolyte.

1.1.3 Mechanism

The DNA strand, the probe, migrates through the capillary tube as a random coil under the influence of the electric field. In the absence of any interaction with the neutral obstacle polymer, the host, it will continue onward in the free-draining limit. When the probe contacts a host polymer it may either form an entanglement or glance off to a side. The forming of an entanglement requires the probe to change its shape and it is these shape-changing encounters which are essential to size dependent separation. Simple transient entanglements between DNA and HEC molecules without changing the DNA shape and breaking its spherical symmetry are not effective in introducing size dependence of electrophoretic mobility.[10,11] When a shape-changing event occurs, the probe leaves its coiled conformation to instead take on a pulley-like form with two arms, not necessarily of equal length, one on either side of the host polymer. Thus, the probe forms a U-shape about the host. Both of the arms are still being stretched in the forward direction by the electric field, but one arm, most likely the longer arm, is able to pull the

shorter arm to its side. The smaller arm then migrates *against* the electric field and around the point of intersection to the side of the bigger arm. After both arms are free from the entanglement, the DNA probe then returns to its random coiled shape and moves again unimpeded under the influence of the field.

The probe is still advancing through the capillary, though at a much slower rate, during the duration of this entanglement period. The additional frictional drag is a direct result of the probe pulling the neutral polymer along and it is responsible for this decrease in mobility. It is possible that multiple entanglements will be occurring at the same time. This process of coiling – entangling – coiling repeats itself as the probe migrates through the capillary tube. A larger probe strand has a higher probability of encountering a host polymer and having an entanglement. In addition, a larger probe will take longer to release itself from the entanglement; the amount of time spent with the reduced velocity is therefore higher for longer DNA molecules. The mobility of the DNA is certainly a function of its molecular weight and this allows for size-dependent separation.

Barron[1] presents the following argument for understanding the process of entanglements in dilute polymer systems. Consider a freely orienting polymer with N subunits. The diffusion coefficient D is the ratio of $k_B T$ to some molecular friction factor. Allow f_0 to represent the amount of force needed to pull one subunit though the capillary with a unit velocity. This f_0 is a force divided by a unit velocity – it carries the same units as a drag coefficient (mass per time). The total drag coefficient for the polymer with N subunits is then Nf_0. In this case the diffusion with no entanglements is

$$D = \frac{k_B T}{N f_0} \tag{1.1}$$

If the probe polymer were entangled with a host polymer, a force greater than Nf_0 would be required to maintain the particular velocity. As the electric field remains constant, the force on the probe polymer is unchanged. The effect of this entanglement is that the probe polymer cannot maintain the particular velocity. It is slowed down by the entanglement. Notice that the increase in force required is related to N. The longer polymer will have more entanglement points and it will advance more slowly through the solution.

1.2 PREVIOUS WORK

1.2.1 Experimentation

Barron[1] first determined the entanglement threshold for different molecular weight fractions of HEC. She defined Φ^* as the concentration at which polymer chains begin to overlap and interaction first appears. In a plot of the specific velocity (η_{sp}) of the solution versus the polymer concentration (Φ) the concentration where the slope significantly changes is Φ^*, the concentration at network formation. Other work went on to show explicitly that size dependent-separation is achieved using HEC as the sieving medium at concentrations well below the threshold limit.

Both solutions are successful is separating the DNA fragments according to molecular weight. This shows that a definite mesh-like sieve is not a required component for capillary electrophoresis of DNA. Barron[1] also found that a low concentration of high MW HEC polymers worked better for separation of long DNA fragments than a high concentration of low MW HEC polymers. If the HEC molecules are too small, during their interactions with the probe they are unable to form the long lasting firm entanglements that significantly hinder the probe motion.

One method to gain a quantitative measure of the dynamics of the probe-host interactions is to treat the DNA coil as an ellipsoid and monitor the changes in the three principle radii $\left(R_x, R_y, R_z\right)$. R_x is the radius in the flow direction. A second technique is to evaluate the velocity of the center-of-mass of the probe $\left(v_{cm}\right)$. When the probe is involved in an entanglement the usual random coil shape is replaced by the U-shape conformation. The value of R_x is significantly larger in this formation than in the transient flow because the two extended arms are contributing to the radius. v_{cm} is constant for a probe advancing without entanglement. It is considerably slowed during a period of interaction by the increase in hydrodynamic resistance from the host polymer. Both v_{cm} and R_x return to their previous static values following an entanglement event.

1.2.2 MD and BD Simulations

Computer simulations offer an excellent opportunity to study the dynamics of entanglements of polymers in dilute solutions. The model system can be designed to

include a probe DNA chain and a number of host polymer chains. Recall that some of the advantages of the dilute solution included avoiding simulation of the entire gel network and a lesser amount of time spent doing intensive interaction calculations. Various simulation ideals are available including molecular dynamics (MD) and Brownian dynamics (BD).

In an MD simulation[17,18,19,20] Newton's equations for motion are solved directly for each monomer for each small step forward in time. To maintain conservation of energy and momentum it is necessary to simulate the entire space. There must be an available exchange with the surroundings. The solvent surrounding the polymer must therefore be included in the simulation, and it must be allowed to interact. Typically, twenty times as many solvent molecules are needed per monomer in the chain.[18] The explicit motion of the solvent is not relevant to the interaction dynamics, and the inclusion of these calculations in the algorithm makes it so inefficient that MD is rarely used for chains of substantial length.

The solvent is replaced by a continuum in a BD simulation. Each monomer, or each bead consisting of multiple monomers, feels a random force at each time step that simulates the effects of collisions with solvent molecules. This Brownian force is defined to have an ensemble average of zero and should have no overall effect on the motion of the polymer chain. This tenet of BD gives it a considerable advantage over MD in that only the motion of the monomer pieces needs to be calculated at each time step.

It is assumed that the polymer strand can be simplified into a chain consisting of beads connected by sticks. The beads represent points along the chain where the polymer feels the force from its environment that causes it to translate or change orientation. All the force is concentrated on these beads, and the connecting sticks do nothing more than hold the beads together. The sticks are free to rotate about the beads to which they are connected and this permits the chain to sample various conformations.

The next level of simplification of the BD method deals with the coarse-graining procedure. The simulation needs to be accurate only to the length and time scales consistent with the physics of the problem to be solved. One extreme is the pearl necklace approach where each individual monomer is represented by a bead. A polymer of 100000 monomers would consist of 100000 beads. The length of the connecting sticks is such that the product of the length of the stick and the number of sticks equals the fully stretched length of the polymer. This scaling requires the use of many beads and relatively short sticks. This is too simplistic a process to portray detailed chemical structure, but it does do well to mimic some primary characteristics of the chain.

For problems with a larger length scale it is common to use fewer beads and longer sticks to model the same length polymer chain. If the motion of distinct monomers is not required then a number of monomers can be grouped together into one bead. The distance between each bead (the length of the stick) is fixed at one Kuhn step. The Kuhn step is a characteristic length specific to the polymer chain. The length of the Kuhn step will set the number of monomers that can be grouped in each bead. The distance

between each bead can be greater than that used in the pearl necklace method. This is the bead-rod approach to BD. During the simulation is it important to ensure that the length of each rod remains the same. This scaling requires fewer beads than the pearl necklace method.

The highest level of simplification again decreases the number of beads and increases the length of the connections. In this case each bead may represent 10000 monomers, and the rod connecting each bead would then need to be 10000 times as long as in the pearl necklace. This rod must now be given an increased degree of flexibility to continue to accurately model the polymer. The rod is replaced by a spring that is allowed to shrink and extend at each time step. Each spring has a maximum extended length, defined such that the fully stretched length of the polymer is still unchanged, and it is an important part of the simulation to ensure that no spring is ever over-extended. The advantage of the bead-spring BD simulation is that it can model a long polymer chain with the fewest number of monitored points.

A key assumption in BD is that intermolecular forces between macromolecules are neglected. There is no bead-to-bead potential and the beads do not sense their nearness to one another during the simulation. The springs only exist to connect the beads; they do not exist in the sense of occupying any space and so they are "phantom springs"; any two springs may pass through one another. Each move forward in time is uncorrelated with the previous move. There is no information from timestep t that is used to determine the direction or speed of move $t + \Delta t$.

At each timestep there are three forces acting on each bead. The Brownian force represents the effects of the solvent molecules. The drag force relates the velocity of the beads to the velocity of the solvent

$$\mathbf{F}_{drag} = \zeta\left(\mathbf{V} - \dot{\mathbf{r}}\right) \tag{1.2}$$

where ζ is the drag coefficient, $\mathbf{V}$ is the velocity of the solvent at the bead location, and $\dot{\mathbf{r}}$ is the velocity of the bead $\left(d\mathbf{r}/dt\right)$. The drag coefficient is determined based on diffusivity measurements and polymer theory, and it is a function of the length of the molecule, the viscosity of the solvent, and the number of model beads used.[22] The spring force is a function of the extension of the spring and is used to maintain that no spring is ever over-extended. The location of the bead after a timestep is directly of function of the combination of these forces.

BD assumes that no acceleration occurs during the small increment of the timestep. The inertia is negligible because the mass of any individual bead is near zero. A second assumption is that over the timestep the forces acting on any bead remain constant. It is then simple to rearrange the force balance to get an equation relating the velocity of the bead to the Brownian and constraint forces.

$$\sum \mathbf{F} = m\mathbf{a} = 0 \tag{1.3}$$

$$\mathbf{F}_{drag} + \mathbf{F}_{spring} + \mathbf{F}_{Brown} = 0 \tag{1.4}$$

$$\frac{d\mathbf{r}}{dt} = \mathbf{V} + \frac{\left[\mathbf{F}_{spring} + \mathbf{F}_{Brown}\right]}{\zeta} \tag{1.5}$$

Given a velocity field and a timestep, this process can be solved using first order Euler integration to determine the new position of each bead following each move.

1.2.3 Previous Simulation Work

Some simulation work has previously been done investigating the dynamics of a polymer strand encountering an obstacle. Sevick and Williams modeled a polyelectrolyte collision with a post in a microlithographic array.[7] Nixon and Slater used BD to simulate two-dimensional DNA electrophoretic collisions with a single non-moving obstacle.[4] Starkweather et al have used Monte Carlo simulations to study single chain entanglement in dilute solution capillary electrophoresis.[3] These works are the beginning of understanding the mechanism of interaction.

Sevick and Willams[7] believed that the separation achieved from driving a charged polymer through a dilute polymer solution might also be accomplished by replacing the solution with a random array of posts. They used lithographically etched arrays of silicon as the electrophoretic medium. The polyelectrolyte assumed the form of having two arms of the chain extended along either side when it contacted a post, as was predicted by Barron.[1] It is significant to note that if the radius of gyration of the polymer in the flow

direction is larger than the spacing between posts in this grid array arrangement then simultaneous interactions with multiple posts is possible.

A two-dimensional BD algorithm was used to simulate an electrophoretic collision between a bead-spring polyelectrolyte and a stationary circular obstacle. A soft-core repulsive potential was introduced between the beads and the obstacle. Nixon and Slater[4] began their simulation with the DNA molecule confined to a narrow channel and flowing toward the obstacle. The molecule obeys the traditional dynamics of a free-draining coil in the absence of any collisions. It is not possible for the DNA to avoid the post by passing above or below it because this is a two dimensional simulation. The radius of the obstacle was chosen such that $R_{obs} = L/2$ (with L as the spring length). This ensured that, even if the spring was fully stretched, the DNA could not pass through the post without the bead-post repulsive force taking effect. This simulation was designed to guarantee a collision for each trial.

Figure 1.1 clearly illustrates six instances during one particular trial. The DNA molecule begins upstream of the post, (a). It has no knowledge of the obstacle and it travels forward in a random coil conformation. When a collision occurs, (b), the DNA is unable to pass by the post if it remains in its coiled orientation. The electric field continues to drive the DNA forward. This driving force is strong enough to compel the polymer to change its form and adapt the U-shape structure with two arms, (c, d), one reaching out on either side of the post. The longer arm continues to grow at the expense of the shorter

arm, and eventually the entire polymer collects on one side, (e), and passes the obstacle. Downstream of the post, (f), the DNA begins to return to its random coil configuration.

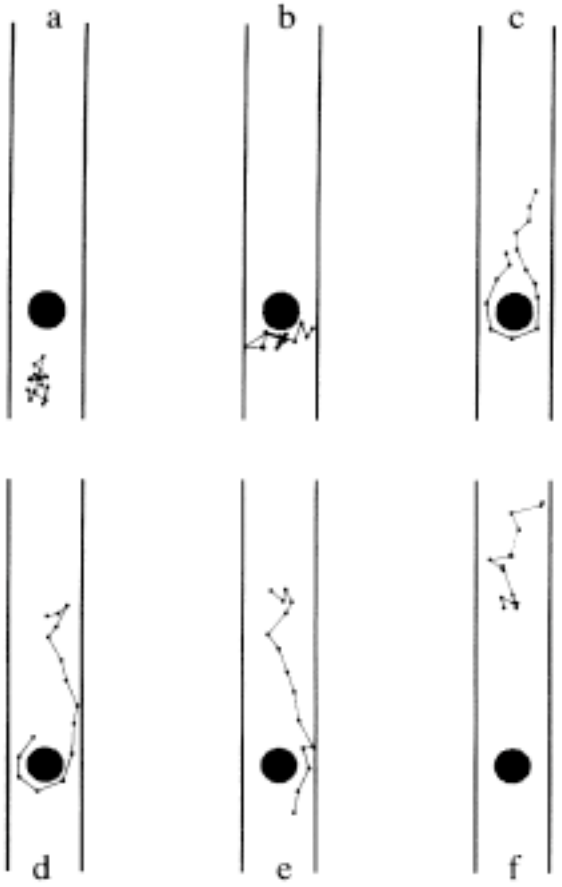

FIGURE 1.1 Simulation snapshots of the collision between a charged bead-spring polymer and a circular obstacle. This figure is from [4].

The ensemble-averaged position of the center of mass, $\langle y(t) \rangle$, advances down the length of the column with time. (Nixon and Slater define the y-direction to be parallel to the tube axis.) Figure 1.2 indicates that, both before and after the collision, $\langle y(t) \rangle$ moves with a constant velocity. This velocity is significantly retarded during an interaction because the molecule must take time to undergo the shape-changing conformation. The average time delay due to entanglement was ~3.4 time units. They also present the changes in the two mean square end-to-end distances. Figure 1.3 shows a small increase in R_x and a much larger increase in R_y. The DNA experiences three stages during the collision. The first stage is a "stacking" stage[4] where the polymer contacts the post and spreads out in the column – this is responsible for the change in R_x. It then stretches out the two arms – the significant change in R_y – in the flow direction, and then finally returns to its coiled form. The cyclic process of coiled-stretched-coiled is not periodic. Notice that even after the probe is free from its entanglement $(t \approx 25)$ the displacement in R_y has not returned to its pre-interaction value. There is a duration following release during which the probe remains distorted from its random coil form.

Two factors are important for the success of a dilute polymer solution in capillary electrophoresis. It is necessary to maximize the molecular-size-dependent retardation due to the sieving process of collisions between the migrating molecules and the separation matrix. In addition, it is imperative to minimize the dispersion of molecules due to these collisions.[4] Nixon and Slater conclude that single entanglements between DNA molecules and dilute polymers would be insufficient for successful electrophoresis. They believe the escape process from the collision is not detailed enough for efficient

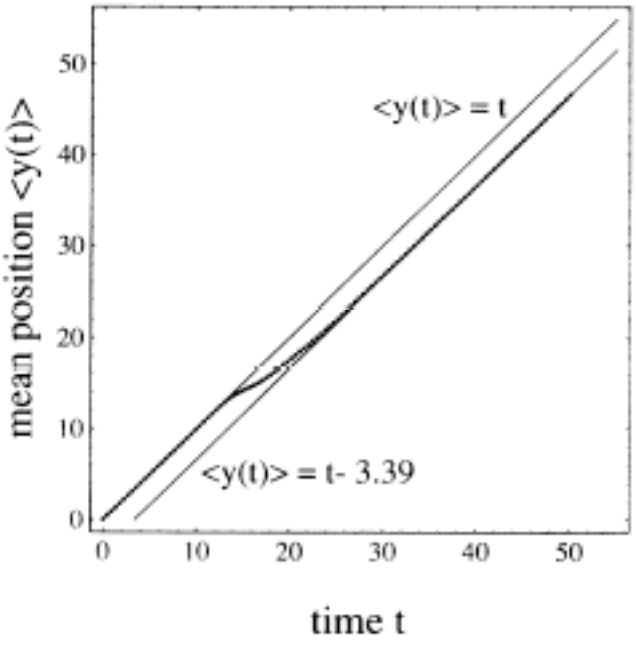

FIGURE 1.2 The mean position of the center of mass along the tube axis vs. time for a population of 867 molecules. This figure is from [4].

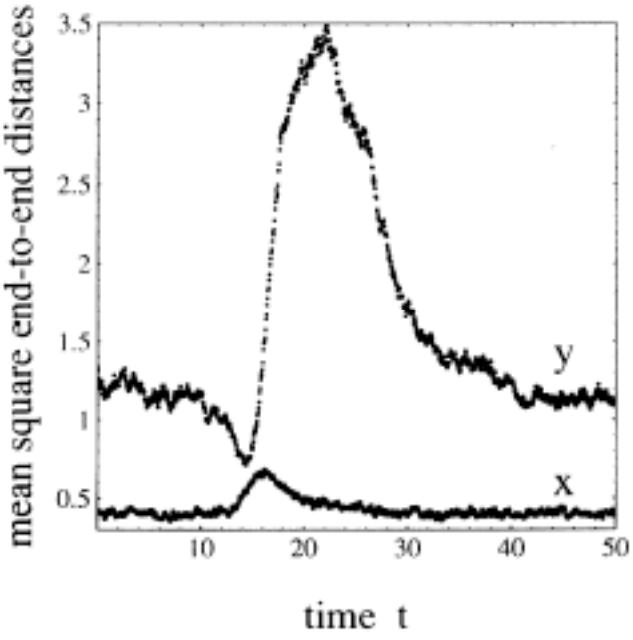

FIGURE 1.3 Mean squared end-to-end distance vs. time. The *y*-direction is parallel to the tube axis. This figure is from [4].

separation and that the large range of escape times leads to increased molecular diffusion. They argue that multiple collisions are necessary, and therefore the use of a dense gel media in the capillary is required.

The work of Starkweather[3] et al uses a Monte Carlo simulation procedure on a pearl necklace representation of the polymer chain. Each bead in the chain is given a hard sphere potential and a radius α large enough to prevent bond crossings.

$$V(r) = \begin{cases} 0 & if\ r > \alpha \\ \infty & if\ r \le \alpha \end{cases} \tag{1.6}$$

The obstacle is also represented by a pearl necklace chain with the hard sphere potential (different from the 2D post used by Nixon[4]). This simulation is performed in three dimensions so it allows for the possibility that the probe may pass by the host without interaction.

The host chain is first equilibrated and then its orientation and location are frozen for the remainder of the simulation. The probe chain is also equilibrated and then it is placed a fixed distance upstream of the host. The probe, driven by the electric field, migrates away from its original position and may interact with the host. An entanglement is signified if the probe strongly deforms in the field direction. The probe may miss the host entirely, it may contact it but glance off to one side, or it may become fully entangled. The first case shows no time delay, the second may slow the probe but without significant conformation change, and the third results in both a large time delay

and orientation alteration. It is this third engagement that is most important to size dependent separation. Figure 1.4 demonstrates the motion of the probe during a fully developed entanglement.

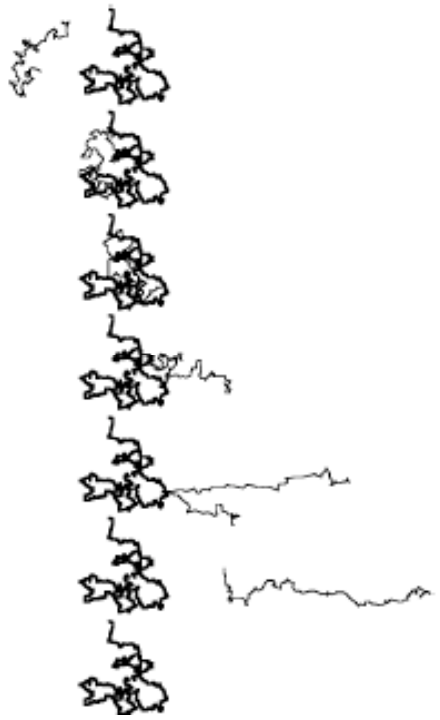

FIGURE 1.4 This shows the typical time evolution of conformation for a probe chain in the strong entanglement case. Notice the two arms. This figure is from [3].

Starkweather[3] compares the center-of-mass movements of a simulation featuring a high level entanglement against a simulation that avoided entanglement. They shows that, similar to what Nixon[4] found in the 2D case, during interaction the otherwise constant advancement of the polymer is strongly retarded from its free-draining motion. They find

that the slope of the non-interacting polymer is comparable to that of the interacting polymer following its entanglement.

Starkweather concludes "the interaction of a mobile polyelectrolyte chain and a single neutral host can endow the polyelectrolyte with a strongly molecular-weight-dependent mobility, even in the absence of host mobility."[3] This is exactly opposite to the belief presented by Nixon and Slater.[4] The mechanism explaining entanglement dynamics between probe and host continues to be unclear, and the use of dilute polymer solutions in capillary electrophoresis remains a field to be explored.

REFERENCES

[1] Barron, A.E.; Soane, D.S.; Blanch, H.W. *Journal of Chromatography A* **1993**, *652*, 3.

[2] de Carmejane O *Graduate Thesis – University of Michigan* **2001**.

[3] Starkweather, M.E.; Muthukumar, M.; Hoagland, D.A. *Macromolecules* **1998**, *31*, 5495.

[4] Nixon, G.I.; Slater, G.W. *Physical Review E* **1994**, *50(6)*, 5033.

[5] Ogston, A.G. *Transactions of Faraday Society* **1958**, *54*, 1754.

[6] Grossman, P.D. *Biopolymers* **1991**, *31*, 1221.

[7] Sevick, E.M.; Williams, D.R.M. *Physical Review Letters* **1996**, *76(14)*, 2595.

[8] Strege, M. *Analytical Chemistry* **1991**, *63*, 1233.

[9] Li, L.; Larson, R.G.; Sridhar, T. *Journal of Rheology* **2000**, *44(2)*, 291.

[10] Morris, M.; Shi, X.; Hammand, R.W. *Analytical Chemistry* **1995**, *67(6)*, 1132.

[11] Somasi, M; Khomami, B.; Woo, N.J.; Hur, J.S.; Shaqfeh, E.S.G. *Journal of Non-Newtonian Fluid Mechanics* **2002**, *108*, 227.

[12] Morris, M; Shi, X.; Hammand, R.W. *Analytical Chemistry* **1995**, *67(18)*, 3219.

[13] Beebe-Poli, J. *Analytical Chemistry* **1992**, *64*, 896.

[14] Viovy, J.C. *Electrophoresis* **1993**, *14*, 322.

[15] Duke, T.A.J. *Physical Review Letters* **1992**, *69*, 3260.

[16] Hubert, H.J. *Macromolecules* **1996**, *29*, 1006.

[17] Everears, R; Kremer, K.; Grest, G. *Macromolecular Symposium* **1995**, *93*, 53.

[18] Grest, G.; Kremer, K. *Physical Review A* **1986**, *33(5)*, 3628.

[19] Kremer, K.; Grest, G. *Journal of Chemical Physics* **1990**, *92(8)*, 5067.

[20] Kremer, K.; Grest, G. *Physics World* **1995**, *8(3)*, 39.

[21] Larson, R.G.; Hu, H.; Smith, D.E.; Chu, S. *Journal of Rheology* **1999**, *43(2)*, 267.

[22] Chopra, M.; Larson, R.G. *Journal of Rheology* **2002**, *46(4)*, 831.

CHAPTER 2

USING SPRING REPULSIONS TO MODEL ENTANGLEMENT INTERACTIONS IN BROWNIAN DYNAMICS SIMULATIONS OF BEAD-SPRING CHAINS

We develop a bead-spring Brownian dynamics model for simulating the topological interactions between polymers and thin obstacles, and apply this method to electrophoretically translating DNA strands interacting with an immovable post. The use of a bead-spring method allows for the simulation of entanglement interactions of polymer chains too long to be simulated using bead-rod or pearl necklace models. Using stiff "FENE-Fraenkel" springs, we are able to model short chains as well. Our new method determines the shortest distance between a spring and the post, calculates a repulsive force inversely related to this distance using an exponential potential, and corrects for the rare situation when a spring passes beyond the post despite the repulsive interaction. As an example problem we consider single-chain collisions with a single post in weak electric fields. We explore a wide range of chain lengths (25 Kuhn steps – 1515 Kuhn steps) and we find that the average delay produced by the collision is a function of both the chain length and the Peclet number. Chains of all lengths reach the same upper limit at high Peclet number but they follow separate curves with similar slopes at lower Peclet number. Our results are consistent with published results for a 25

Kuhn-step chain at Peclet number $Pe = 1.0$. Our new method is a general one that allows us to compute the effects of entanglements in systems with rare entanglements and long chains that cannot be simulated by other more microscopic methods.

2.1 INTRODUCTION

There are a number of problems in polymer physics where rare entanglements dominate, and these problems cannot be addressed by traditional methods such as "tube models" and fine-grained simulations that assume entanglements are dense or chains are short. Problems in which rare entanglements are important include the dynamics and rheology of semi-dilute solutions of long polymers and electrophoresis of DNA in dilute polymer solutions through arrays of posts. While we focus here on the latter problem, the methods we develop could be applied to other situations dominated by rare entanglements.

Size-dependent separation of DNA polymer strands has useful applications in medical diagnostics, drug development, forensics, and gene therapy[1]. A common process to separate DNA strands uses capillary electrophoresis through a solution of neutral obstacles. The neutral objects could be other polymer molecules either in a cross-linked gel or in solution[2], or micro-fabricated thin posts in a microchannel[3,4,5]. When a DNA strand is blocked by a post or gel filament, the DNA leaves its coiled conformation to take on a pulley-like form with two arms, not necessarily of equal length, one on either side of the obstacle, forming a U-shape or J-shape about the post. Both of the arms are

stretched in the forward direction by the electric field, but one arm, most likely the longer arm, is able to pull the shorter arm *against* the electric field and around the post to the side where the bigger arm resides. After both arms are free from the entanglement with the post, the DNA returns to its randomly coiled shape and moves again unimpeded under the influence of the field. There is a time penalty associated with these interactions – a long polymer takes more time to maneuver around the post than does a short polymer. It is interactions of this type that lead to the size-dependant separation of DNA polymer strands.

A number of simulation methods are available to model this situation. Starkweather[6] et al. studied single chain entanglements in dilute solution capillary electrophoresis. Their Monte Carlo simulation procedure uses a pearl necklace representation of the polymer chain and each bead in the chain is given a hard sphere potential and radius large enough to prevent crossings. Saville and Sevick[17] study a field-driven polymer chain colliding with a finite-sized obstacle. They discuss the "unhooking" and "rolling off" mechanisms for chain release. Nixon and Slater[7] use bead-rod Brownian dynamics (BD) to simulate two-dimensional DNA electrophoretic collisions with a single non-moving obstacle. Their simulation begins with the molecule confined to a narrow channel and flowing toward the obstacle. The radius of the obstacle is chosen such that $R_{obs} = L/2$ (where L is the length of one rod). This ensures that the DNA cannot pass through the post without the bead-post repulsive force taking effect. Patel and Shaqfeh[8] also use a similar bead-rod Brownian dynamics method to model the electrophoresis of DNA through dilute post arrays. They simulate chains of 25 and 150 Kuhn steps. The work of Randall and

Doyle[18] shows experimentally the interactions of polymer chains with a stationary obstacle.

One limitation of such bead-rod or pearl necklace simulations is in the length of chain that can be modeled. The required number of beads must equal the number of Kuhn steps because the length of each rod is fixed at one Kuhn step. Bead-spring BD simulations are more coarse-grained and allow for the simulation of much longer chains since each spring can represent many Kuhn steps. The use of bead-spring BD to solve the polymer/post interaction or other entanglement interactions represents a new approach to such problems. Previous work has generally not considered simulations of bead-spring chains because they do not readily enforce the topological interactions between the polymer and the post. When there is more than one Kuhn step between each bead, bead-post repulsion (used by Nixon & Slater and Patel & Shaqfeh) does not prevent the chain from passing through the post. We here develop a method to apply a repulsive force between each spring and the post. Kumar and Larson[9] proposed such an approach earlier but their algorithm was not able to ensure that the spring did not violate the topological restrictions without reducing the time step size to an unacceptably small value. Here we improve on the method of Kumar and Larson by developing a procedure to determine if any spring has passed through the post and correct those springs as necessary. We are also able to implement in our method the fast predictor-corrector time-stepping method of Somasi et al[13]. We are thereby able to model chains much longer than those in the current literature.

We note here that, for a coarse-grained simulation of polymer melts, Padding and Briels have proposed a related method for imposing entanglement constraints, in which a spring is allowed to "bend" around an entanglement point and the resulting increased spring length generates the forces needed to preserve the entanglement interaction[15]. At this point it is not clear whether or not this method can be adapted to the case of rare entanglement that we are addressing here.

2.2 METHODS

2.2.1 Brownian Dynamics

The simplest bead-spring Brownian dynamics simulations use three forces to move the beads during each time step. The Brownian force represents the random effects of the solvent molecules. This force is given by[10,11]

$$\mathbf{F}_{Brownian} = \left(\frac{6\, k_B T\, \zeta}{\Delta t} \right)^{1/2} \tag{2.1}$$

The drag force relates the velocity of the beads to the velocity of the solvent where $\zeta = \zeta_{tot}/N$, and ζ_{tot} is the drag coefficient for the entire chain, N is the number of beads in the chain, $\mathbf{V}$ is the velocity of the solvent at the bead location, and $\dot{\mathbf{r}}$ is the velocity of the bead $\left(d\mathbf{r}/dt\right)$.

$$\mathbf{F}_{drag} = \zeta\left(\mathbf{V} - \dot{\mathbf{r}}\right) \tag{2.2}$$

The drag coefficient can be determined using diffusivity measurements and polymer theory, and it is a function of the length of the molecule, the viscosity of the solvent, and the number of model beads used[10]. Hydrodynamic interactions between beads are neglected here.

The spring force is a function of the extension of the spring and is used to guarantee that no spring is ever over-extended. We use the worm-like chain version[10,12] of the spring force in our simulation when we model chains long enough that the number of Kuhn steps per spring is greater than 15.

$$\mathbf{F}_{spring\,WLC} = \frac{k_B T}{\lambda_p}\left(\frac{1}{4}\left(1-\frac{|\mathbf{R}|}{R_0}\right)^{-2} - \frac{1}{4} + \frac{|\mathbf{R}|}{R_0}\right)\left(\frac{\mathbf{R}}{|\mathbf{R}|}\right) \tag{2.3a}$$

$k_B T$ is the Boltzman thermal energy factor, λ_p is the persistence length (equal to one half of the Kuhn step length b_K), $\mathbf{R}$ is the end-to-end vector of a spring, and R_0 is the maximum extended length for any spring.

We use the FENE-Fraenkel spring law[16] to model short chains in which each Kuhn step length is represented by a single stiff spring with non-zero minimum length that behaves in a rod-like manner.

$$\mathbf{F}_{spring\,FF} = \frac{k_B T}{\lambda_p}\left(\frac{H\left(|\mathbf{R}|/R_0\right)}{1-\frac{1-\left(|\mathbf{R}|/R_0\right)}{s^2}}\right)\left(\frac{\mathbf{R}}{|\mathbf{R}|}\right) \tag{2.3b}$$

H is the spring constant and s is the extensibility parameter that defines the maximum possible deviation between the actual spring length and the natural spring length (i.e., the length at which the force is zero).

The location of the bead after each time step is controlled by a combination of these forces.

The calculation of the spring force is one opportunity for Brownian dynamics to capitalize on the development of fast semi-implicit algorithms. The distance between two consecutive beads can never be greater than the fully extended length of the spring that connects them. A predictor-corrector integration scheme such as that of Somasi[13] et al. can be used to avoid this situation. They observe that "the premise of the method lies in the fact that the spring force law for any spring in the chain is either written explicitly (from the previous time step, or from a previous step in the current time step, where the length of the connector is guaranteed to be within the bounds) or solved implicitly through the cubic equation." Two advantages of this scheme are that no Brownian move ever needs to be rejected and that larger time steps can be used with confidence. We use this method in our model for both of the spring force options.

Brownian dynamics methods take advantage of the fact that inertial forces on the polymers are small and therefore the sum of the above forces can be set to zero. A second approximation is that over the time step the forces acting on any bead, except for the spring force, remain constant. It is then simple to rearrange the force balance to get an equation relating the velocity of the bead to the Brownian and constraint forces.

$$\sum \mathbf{F} = m\mathbf{a} = 0 \tag{2.4}$$

$$\mathbf{F}_{drag} + \mathbf{F}_{spring} + \mathbf{F}_{Brown} = 0 \tag{2.5}$$

$$\frac{d\mathbf{r}}{dt} = \mathbf{V} + \frac{\mathbf{F}_{spring} + \mathbf{F}_{Brown}}{\zeta} \tag{2.6}$$

Given a velocity field and a time step, this process can be solved using first order Euler integration to determine the new position of each bead following each move. The method of Somasi et al. corrects this approach by evaluating the spring force at the end of the time step and this prevents over-extending the spring[13].

Bead-spring Brownian dynamics simulations are typically designed using phantom springs – connections between beads that have no properties other than holding the beads together. The beads may move in such a way during simulation that these springs can cross and pass through one another or through other objects in the fluid. It is necessary to correct this flaw if BD simulations are to be used to model polymers undergoing

entanglements with each other or with obstacles such as posts. We choose therefore to include a repulsive force acting on the spring that is combined with the other three traditional forces in BD to better simulate the polymer motion:

$$\mathbf{F}_{drag} + \mathbf{F}_{spring} + \mathbf{F}_{Brown} + \mathbf{F}_{rep} = 0 \tag{2.7}$$

The challenge lies in choosing the form of this repulsive potential, incorporating it into the BD simulation, and monitoring its success.

2.2.2 Repulsive Force

We must choose a form of the repulsive force that increases in magnitude as the separation distance decreases toward zero and is small (relative to the other three forces) when the separation distance is large. Kumar and Larson[9] considered two choices, namely an exponential form

$$U_{rep} = Ae^{(-D/\alpha)} \tag{2.8}$$

and a power-law form drawn from the repulsive part of the Leonard-Jones potential:

$$U_{rep} = 4\varepsilon\left(\frac{\sigma}{D}\right)^{12} \tag{2.9}$$

A and ε are the strengths and α and σ are the ranges (respectively) for these potentials. The repulsive force is given by

$$\mathbf{F}_{rep} = -\frac{\partial U_{rep}}{\partial \mathbf{r}} \tag{2.10}$$

One advantage of the power-law form is that the repulsive force is infinitely large at a separation distance of zero. This guarantees that if the equations are solved accurately the spring will be unable to pass through the post. The disadvantage is that a very large repulsive force (which occurs when the spring is very close to the post) will push two beads quite far away from the remainder of the chain, seriously stretching the spring, and making convergence in that time step difficult to achieve. The simulation will thus often require much smaller time steps whenever a spring is close to the post, which is computationally inefficient.

The exponential form of the repulsive force does not have the same problem since it is finite at a separation distance of zero, but this form permits the spring to pass through the post during a time step. We choose to use the exponential form because it allows for large time steps, but we develop a method to determine if and when a spring is broken and to correct for this, so that topological constraints are still maintained.

Kumar and Larson[9] developed the following procedure to compute the distance of closest approach **D** between each spring and the post. Let $\mathbf{P_1}$ be a vector giving the length and direction from some defined origin to the midpoint of any spring. $\mathbf{R_1}$

describes the spring length and orientation. Let t_1 be a scalar that represents a location along the spring with $t_1 = 0$ at the midpoint of the spring and $t_1 = \pm 0.5$ at either end of the spring. We define any point along a spring or post as $\mathbf{P_1} + t_1 \mathbf{R_1}$. The vector of separation between any point on the spring (indicated by 1) and any point on the post (indicated by 2) is

$$\mathbf{D} = \mathbf{P_1} + t_1 \mathbf{R_1} - \left(\mathbf{P_2} + t_2 \mathbf{R_2}\right) \tag{2.11}$$

The distance of closest approach is found by minimizing the magnitude of $\mathbf{D}$ with respect to t_1 and t_2. This requires that

$$\frac{\partial D^2}{\partial t_1} = \frac{\partial D^2}{\partial t_2} = 0 \tag{2.12}$$

where $D^2 = \mathbf{D} \bullet \mathbf{D}$. The solution of equation 2.12 gives the following expressions for t_1 and t_2.

$$t_1 = \frac{\left(\mathbf{P_1} - \mathbf{P_2}\right) \bullet \left(R_2^2 \mathbf{R_1} - R_{21} \mathbf{R_2}\right)}{R_{21}^2 - R_1^2 R_2^2} \tag{2.13a}$$

$$t_2 = \frac{\left(\mathbf{P_2} - \mathbf{P_1}\right) \bullet \left(R_1^2 \mathbf{R_2} - R_{21} \mathbf{R_1}\right)}{R_{21}^2 - R_1^2 R_2^2} \tag{2.13b}$$

where $R_1^2 = \mathbf{R_1} \bullet \mathbf{R_1}$, $R_2^2 = \mathbf{R_2} \bullet \mathbf{R_2}$, and $R_{21}^2 = \mathbf{R_1} \bullet \mathbf{R_2}$.

When $-0.5 \le t_i \le 0.5$ the distance of closest approach lies along the length of the spring or post. When $t_i > 0.5$ or $t_i < -0.5$ the distance of closest approach should be measured from the end of the spring or post (by setting $t_i = 0.5$ or $t_i = -0.5$ as needed). With the correct values for t_1 and t_2 we calculate **D** from equation 2.11.

We calculate a repulsive force from the exponential form and the magnitude of the separation distance vector. This force is applied to the spring, or more precisely, it is applied to the two beads at the ends of the spring. The distribution of the force is determined by the t_1 value for the spring. All of the force is given to bead_i when $t_1 = 0.5$ and all of the force is given to bead_{i+1} when $t_1 = -0.5$. The force is divided proportionally using the lever rule when $-0.5 \le t_1 \le 0.5$. The fraction of the force applied to bead_i is $t_1 + 0.5$ (the remaining fraction applied to bead_{i+1}) with the force being directed along the vector **D** for both beads. This uneven force distribution (it is rare that $t_1 = 0$) causes the spring to rotate because one bead is pushed more aggressively away from the post than the other. This spring rotation is essential for the change of orientation necessary for the polymer to maneuver around the obstacle.

2.2.3 Broken Springs

We admitted previously that the exponential form cannot guarantee that the springs will not pass though the post. Therefore we develop a series of checks to determine when a

spring has made an "illegal" move – i.e., a move that violates the post – and implement an algorithm to correct for these situations in subsequent time steps.

The cross product rule is our initial method of checking for broken springs. We apply this rule to every spring following each time step. Consider two vectors at time i – $\mathbf{R}_i$ and $\mathbf{D}_i$ (the vector along the length of the spring and the separation distance vector) and two vectors at time $i+1$ – $\mathbf{R}_{i+1}$ and $\mathbf{D}_{i+1}$. We determine the two cross product vectors $\mathbf{C}_i = \mathbf{R}_i \times \mathbf{D}_i$ and $\mathbf{C}_{i+1} = \mathbf{R}_{i+1} \times \mathbf{D}_{i+1}$. These represent the cross product *before* the spring moves and the cross product *after* the spring moves. We calculate the dot product between these two cross products $\mathbf{C}_i \bullet \mathbf{C}_{i+1} = |\mathbf{C}_i||\mathbf{C}_{i+1}|\cos\theta$. The move *does not* break a spring if the sign of $\cos\theta$ is positive. The move *does* break a spring if the sign of $\cos\theta$ is negative. We address any broken springs in the next time step. Figure 2.1 shows an example of a broken spring. We do not concern ourselves with the result of the cross product rule for springs that have $t_1 = \pm 0.5$ at the end of a time step – these springs have a shortest distance vector to the post that exceeds the distance to one of their ends and can pass by the post (beside, above, or below) without passing through it (even though the cross product rule may return a negative $\cos\theta$).

We find there are some instances when the cross product rule gives a false positive – it declares a spring as broken when, in fact, the spring did not pass through the post. The most common example of this is when a spring is far from the post where usually the shortest distance vector is to one of the ends of the spring and the result of the cross product rule is disregarded. However, there are rare occurrences (see figure 2.2) when

the spring has an orientation in both time steps for which the shortest distance vector is to the interior of the spring. It is possible that during this time step the spring orientation may adjust in such a way as to result in a negative $\cos\theta$ in the cross product rule but without the spring passing through the post (see figure 2.2). We therefore use a second, more rigorous, method to test springs that fail the cross product rule. This second method confirms or denies the break determined by the cross product rule.

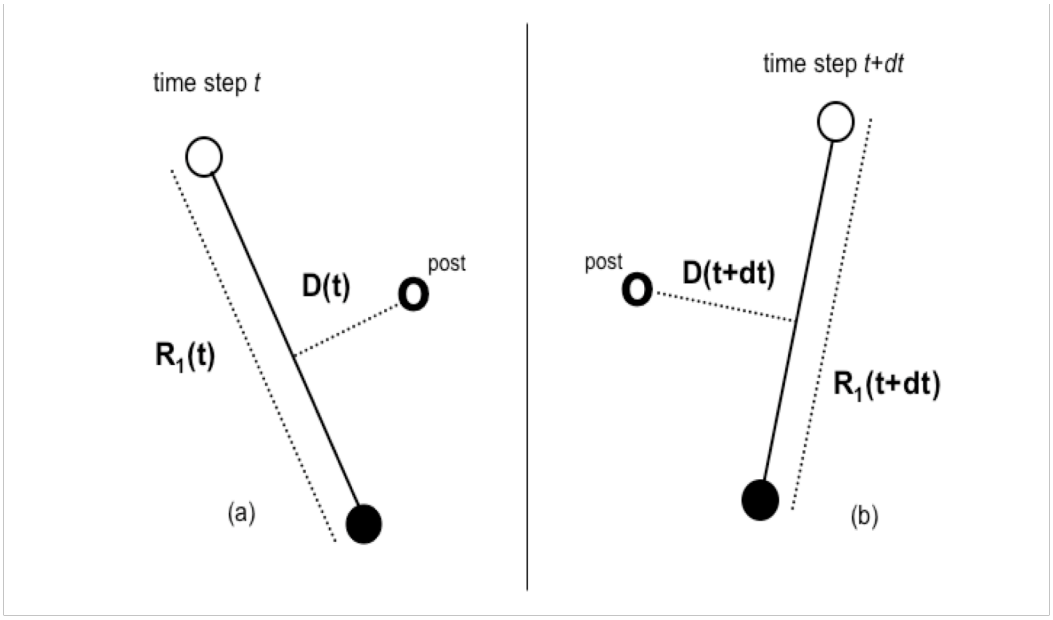

FIGURE 2.1 The cross product rule for detection of a break. The sign of $\mathbf{R}_1(t+dt)\times\mathbf{D}(t+dt)$ is opposite that of $\mathbf{R}_1(t)\times\mathbf{D}(t)$ showing that the movement of the spring from time t to $t+dt$ has broken the post, which is perpendicular to the plane of the page in this example.

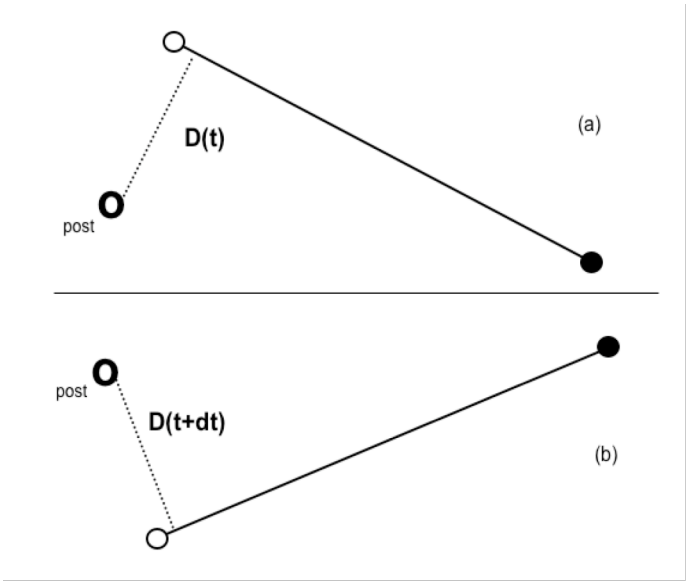

FIGURE 2.2 The cross product rule can give a false positive. This is a case where the spring does not cross the post between time step t and time step $t + dt$.

The second method is the triangle check first discussed by Kumar and Larson[9]. We use the bead locations at two successive time steps to perform the triangle check on a spring that we suspect has broken. We use the positions of bead_i and bead_{i+1} each at times t and $t + dt$ (four pieces of information). We first consider a triangle with corners at $\mathbf{B_i}(t)$, $\mathbf{B_{i+1}}(t)$, and $\mathbf{B_i}(t + dt)$ (see figure 2.3) to illustrate the case when bead_i moves during the time step. If the post is inside this triangle then a crossing occurs. Recall that we describe the line defining the post as $\mathbf{P_2} + t_2\mathbf{R_2}$. The plane that contains the triangle is given by all values of $\mathbf{x}$ satisfying the equation $\left(\mathbf{x} - \mathbf{B_i}(t)\right) \bullet \mathbf{n} = 0$ where $\mathbf{n}$ is the normal vector to the triangle. If we set $\mathbf{x} = \mathbf{P_2} + t_2\mathbf{R_2}$ then the value of t_2 gives the intersection

point of the line containing the post with the plane containing the triangle[9]. The post does not reach the plane if either $t_2 > 0.5$ or $t_2 < -0.5$. There is no break in this case. If $-0.5 \le t_2 \le 0.5$ then the post *does* reach the plane and the post *may* intersect the triangle region but it also might intersect the plane outside of the triangle region.

To determine whether or not the intersection point lies within the triangle we first define three vectors each originating from $\mathbf{B_i}(t)$. The first vector $\mathbf{A}$ is from $\mathbf{B_i}(t)$ to the point where the plane intersects the post. The second vector is $\mathbf{B} = \mathbf{B_i}(t) - \mathbf{B_i}(t + dt)$ (one side of the triangle). The third vector is $\mathbf{C} = \mathbf{B_i}(t) - \mathbf{B_{i+1}}(t)$ (the other side of the triangle). We determine two angles. The first angle, $\angle\mathbf{BC}$, is between $\mathbf{B}$ and $\mathbf{C}$ – this is one of the angles of the triangle. The second angle, $\angle\mathbf{BA}$, is between $\mathbf{B}$ and $\mathbf{A}$ – this is the angle between one side of the triangle and the vector to the post. If $\angle\mathbf{BC} > \angle\mathbf{BA}$ we initially mark this spring as *broken*. If $\angle\mathbf{BC} < \angle\mathbf{BA}$ we initially mark this spring as *not broken*. This is vector set (a) in figure 2.3.

For vector set (b) we repeat this analysis on the same triangle region but we use $\mathbf{B_i}(t + dt)$ as the originating point for all three vectors. We again determine two angles and decide between *broken* and *not broken*. We declare the first triangle is *broken* ONLY when we decide on *broken* for both sets of vectors (a) and (b). Figure 2.3 shows the angles drawn originating from $\mathbf{B_i}(t)$ and $\mathbf{B_i}(t + dt)$ – notice that case (b) is necessary to truly declare this example as *not broken*.

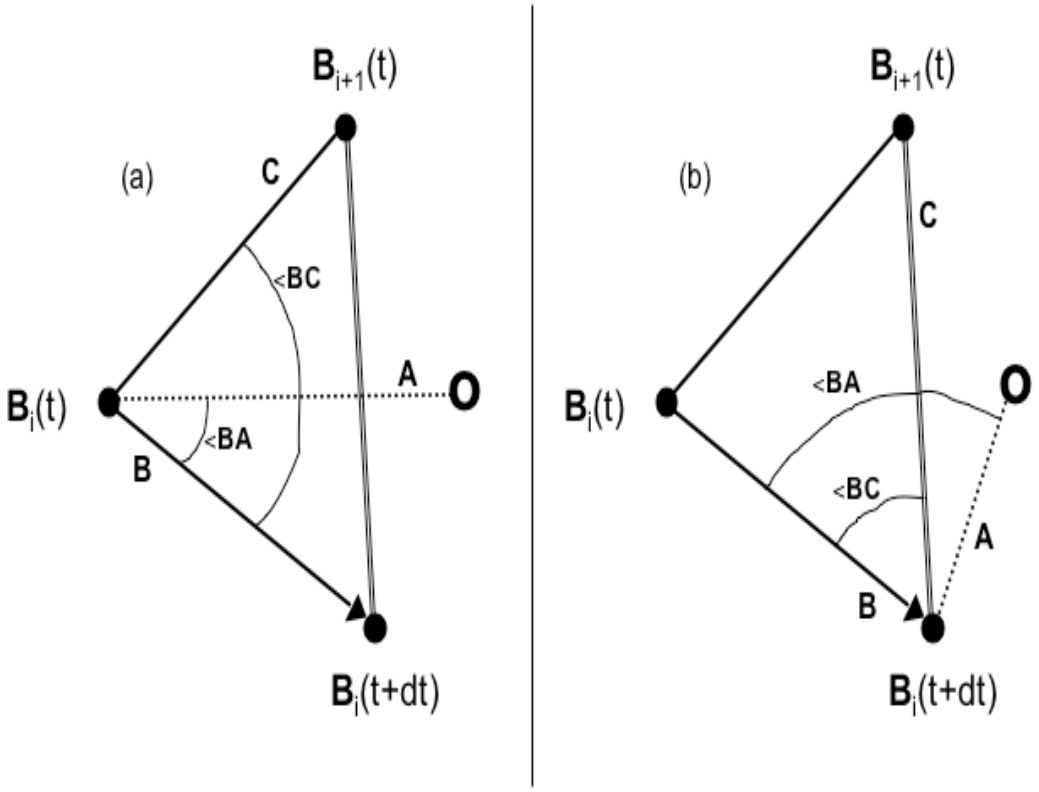

FIGURE 2.3 The triangle rule must originate vectors from two locations – (a) $\mathbf{B_i}(t)$ and (b) $\mathbf{B_i}(t+dt)$. $\angle\mathbf{BC} > \angle\mathbf{BA}$ in (a) – this *may* be a break. $\angle\mathbf{BC} < \angle\mathbf{BA}$ in (b) – confirmation that this is **not** a break.

We perform the same method, with cases (a) and (b) again, a second time for a triangle defined by $\mathbf{B_i}(t+dt)$, $\mathbf{B_{i+1}}(t)$, and $\mathbf{B_{i+1}}(t+dt)$. This triangle allows us to search for breaks that occur when bead_{i+1} moves after bead_i has already moved. We again define a plane by the triangle region and we find the value of t_2 at which this plane intersects the post. We again evaluate two sets of vectors – one set beginning at $\mathbf{B_{i+1}}(t)$ and the other set beginning at $\mathbf{B_{i+1}}(t+dt)$.

The total move is a break ONLY when one triangle region results in *broken* and the other results in *not broken*. If both triangle regions result in *broken* the net effect is NOT a break. In this case the move of the second bead corrects the break from the move of the first bead.

This triangle method is rigorous, and it provides a thorough check of the spring-post interaction. It is easy to see how the cross product rule is a less computationally expensive method. This is why we use the triangle check only in cases when the cross product rule declares a spring as broken.

We accept a move that breaks a spring but we note which (if any) springs are broken during time step t and we attempt to correct those springs during subsequent time steps. We permit breaks to occur temporarily on the grounds that the spring is a coarse-grained object and there is no need rigorously to prevent it from drifting slightly past an entanglement point. The polymer that the spring represents can, in fact, bend somewhat around this point. There are two adjustments we apply to a broken spring to ensure that this break is not "forgotten" by the simulation but that it is eventually repaired. First, we change the sign in the exponent of the repulsive potential from negative to positive. This results in a greater magnitude of the repulsive force for a given separation distance and produces a force that becomes exponentially greater as the separation between the post and the spring increases. Hence, the break generates an even greater restoring force if the broken spring tries to drift away from the post. Second, we change the sign of the

components in the separation distance vector when we use them to determine the direction of the repulsive force. The total effect of these two adjustments is to force a broken spring back past the post with more force than it had in the previous time step. We use the cross product rule and the triangle check at the end of this time step and we usually find that the spring is declared as *broken* again. When a spring is broken in one time step but broken again in the following time step the net result is that the spring is back in a valid location. This is the goal of our method – we allow the break in the first place and then correct it in the next move, or, if necessary, in later moves. In all events the break is remembered and the spring is not allowed to simply drift away from the post until the break is corrected.

One special exception occurs when we pass a break from one spring to the next. A spring may break during time step *t*. The separation distance vector drawn to the spring during time step $t + dt$ may go to one of the two ends of the spring (if $t_1 = \pm 0.5$). In this situation we move the break to an adjacent spring before we apply the two changes discussed earlier. We pass the break to spring *N+1* when $t_1 = 0.5$ (up) and we pass the break to spring *N-1* when $t_1 = -0.5$ (down). If the originally broken spring (at time step *t*) is either the first or last spring in the chain we may pass the break off the end of the chain entirely. An end spring that has a separation distance vector to its open end is able to pass by (or above or below) the post without a true break.

This procedure models in a coarse-grained manner the physics of the chain-post interaction. A spring (or springs in the case when there is a passing) oscillates mildly on

either side of the post as it alternates between *broken* and *not broken* while the other forces continue to change the position and orientation of the spring. This eventually allows the spring to pass the post without a break.

Since our method does not perfectly localize the entanglement interaction, but allows some "slop" in its position that depends on the strength and range of the potential and the number of beads, we need to check that the model can be made insensitive to these non-physical variables. Strength – A in equation (2.8) – relates to the value of the repulsive force when the separation distance is zero. A higher strength produces a greater repulsion between the spring and the post. Range – α in equation (2.8) – relates to the effective thickness of the post. A small range allows the coil to get closer to the post before it begins to feel the repulsion.

2.2.4 Simulation Set-Up and Testing

We first use a polymer with length 100μm for our test simulations. We set the persistence length (λ_p) at 0.066 μm (this gives 379 Kuhn steps of length of 0.132 μm) and we employ a total drag coefficient for the polymer (ξ_{tot}) of 10.0 s/μm^2 that is normalized over one unit of Boltzman energy (k_BT). We choose the initial polymer orientation to be a stretched (39% extension of the full length) nearly vertical line and we place the center of this chain a small distance (about one-third of a Kuhn step) upstream of the post. Figure 2.4 shows a picture of this setup. The purpose of this non-random initial polymer configuration is to maximize the probability and duration of the chain-

post interaction to test and optimize our method of handling coarse-grained spring-post interactions. We employ a coiled start-up condition for other simulations described later. We plot our results for this section as the x-component of the position of the center-of-mass – r_c^x – against time. Each of the four curves (one for each of four strengths) is an average over 100 trials. We generally see three phases in these plots. We see an increase in r_c^x early as the two ends of the chain extend downstream on either side of the post forming a hairpin around the post. Then we see a period of stagnant r_c^x as the chain frees itself from the interaction. Finally we see a constant increase in r_c^x as the chain advances again after it has maneuvered around the post.

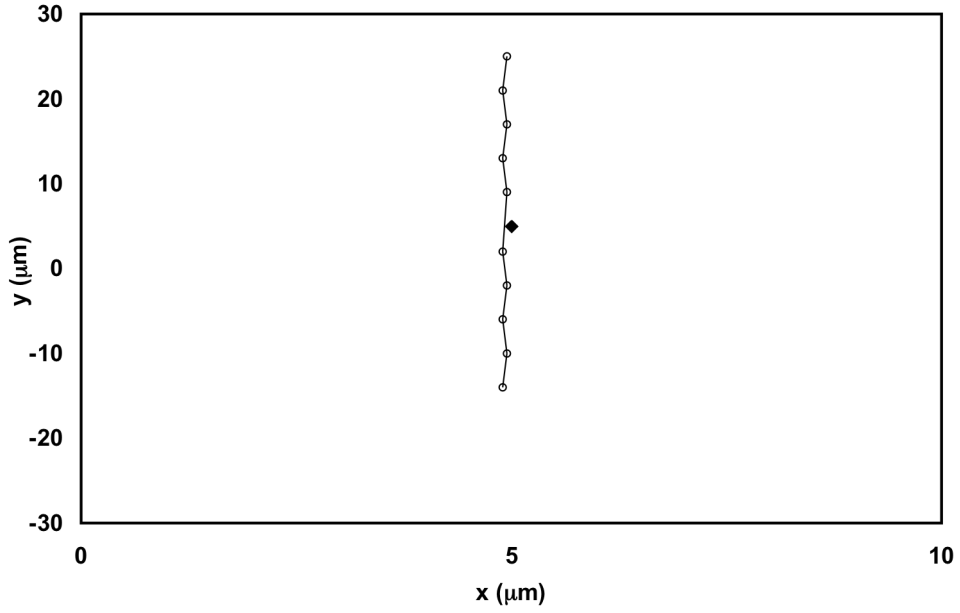

FIGURE 2.4 The initial configuration for the tests of convergence is designed to maximize the probability and duration of entanglements. The post (black diamond) is located at (5,5).

We test 10-bead and 20-bead simulations (both still for the 100 μm long chain) at four different fluid velocities and four choices of strength. The "fluid velocity" here is equivalent to a choice of field strength that would produce that velocity in the absence of the post. Figures 2.5 and 2.6 show results for the 10-bead and 20-bead cases. The fluid velocity is made non-dimensional by the ratio of radius of gyration to relaxation time. Strength (with units of force) is made non-dimensional with $k_B T/\lambda_p$. Range (with units of length) is made non-dimensional by the radius of gyration (R_g) of the polymer coil. The choices of non-dimensional strength vary by a factor of eight (50, 100, 200, and 400). We determine the velocity at which we are no longer able to achieve convergence among the strengths. This is significant because strength is an arbitrary parameter introduced into our simulations by way of our choice of modeling the repulsion between the polymer and the post. We are confident in our simulations only in the regimes where our results are insensitive to value of this parameter. We learn that more beads are necessary to reach convergence at higher fluid velocities.

Non-dimensional fluid velocity, $\overline{V} = \dfrac{V}{\left(R_g/\tau\right)}$ (2.14)

Non-dimensional strength, $\overline{A} = \dfrac{A}{\left(k_B T/\lambda_p\right)}$ (2.15)

Non-dimensional range, $\overline{\alpha} = \dfrac{\alpha}{R_g}$ (2.16)

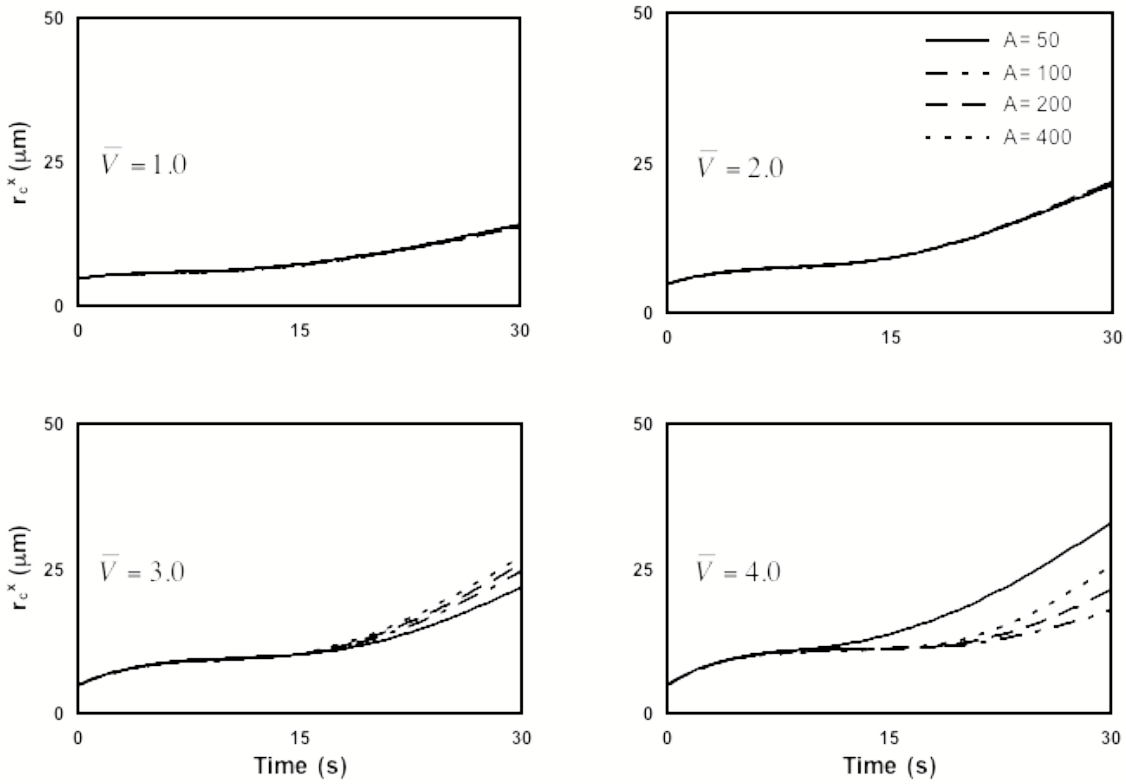

FIGURE 2.5 Center of mass versus time for an initially straight 100 μm chain placed a distance 0.05 μm upstream from the post. This uses 10 beads and non-dimensional strengths of 50 / 100 / 200 / 400 with four non-dimensional fluid velocities ($\overline{V}$) with $\overline{\alpha} = 0.0540$ and time step Δt = 0.0020. Notice that the convergence fails at $\overline{V} \geq 3.0$.

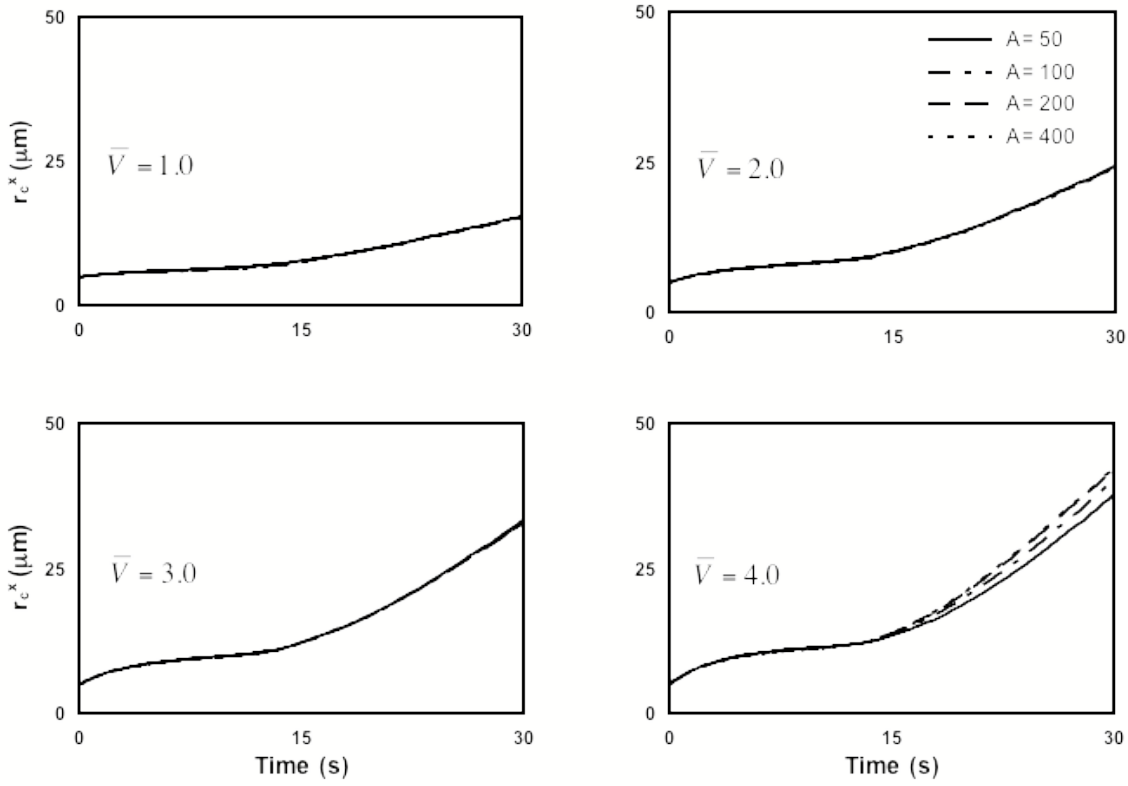

FIGURE 2.6 The same as figure 2.5 but with 20 beads. Notice that convergence is achieved at $\overline{V} = 3.0$ but is not achieved at $\overline{V} = 4.0$.

The choice of range must lie between two extremes. A range that is too large results in an effectively "fat" post – the chain is unable to get close enough to form the hairpin orientation; instead the entire coil is bounced off to one side. There is minimal separation effect without the hairpin formation. A range that is too small can also result in a "fat" post since the chain can greatly overshoot the post, breaking the spring, before the repulsive force begins to take effect. There are thus too many spring-post violations when we use too small of a range. We find through our simulations that a non-dimensional range of 0.0540 gives the best results. This is where we see physically meaningful data that has no dependence on the choice of $\overline{A}$. In real dimensions, for the 100μm chain, this range is equal to 0.08008 μm, which is a bit more than one-half of a Kuhn step. This produces a sufficient degree of localization for our coarse-grained model.

We also perform tests with the 100μm chain using a random coil as the initial configuration, where the random coils are obtained by relaxing the chains for several relaxation times in the absence of the post. This is the starting orientation used by Patel and Shaqfeh[8]. We see fewer hairpin collisions than with the straight chain because the polymer can more easily pass the post without leaving its coil formation. We again see the relationship between fluid velocity and required number of beads. However, with this random initial configuration, figure 2.7 shows that we are able to reach higher $\overline{V} = 4.0$ using 20 beads – only at $\overline{V} = 6.0$ do we fail to reach convergence among the choices of strength. Figure 2.8 shows convergence with the number of beads (10, 20, and 40) at $\overline{V} = 3.0$. Finally, we also varied the time step and reached convergence for both 10-bead

($\Delta t = 0.0020$ and $\Delta t = 0.0040$) and 20-bead ($\Delta t = 0.0005$ and $\Delta t = 0.0010$) simulations. These non-dimensional time steps (made so using the relaxation time) are typical for Brownian dynamics simulations.

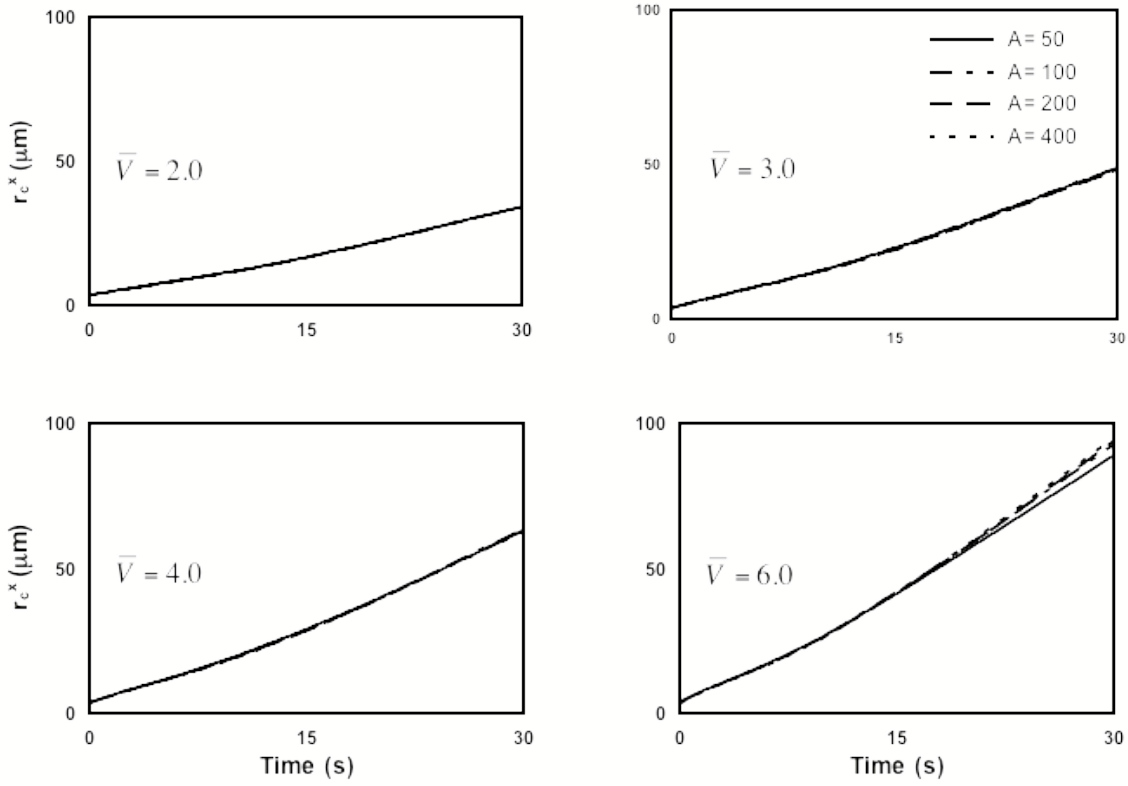

FIGURE 2.7 The same as figure 2.6 except the initial chain configuration is a random coil. Convergence is now obtained at $\overline{V} = 4.0$ and 20 beads.

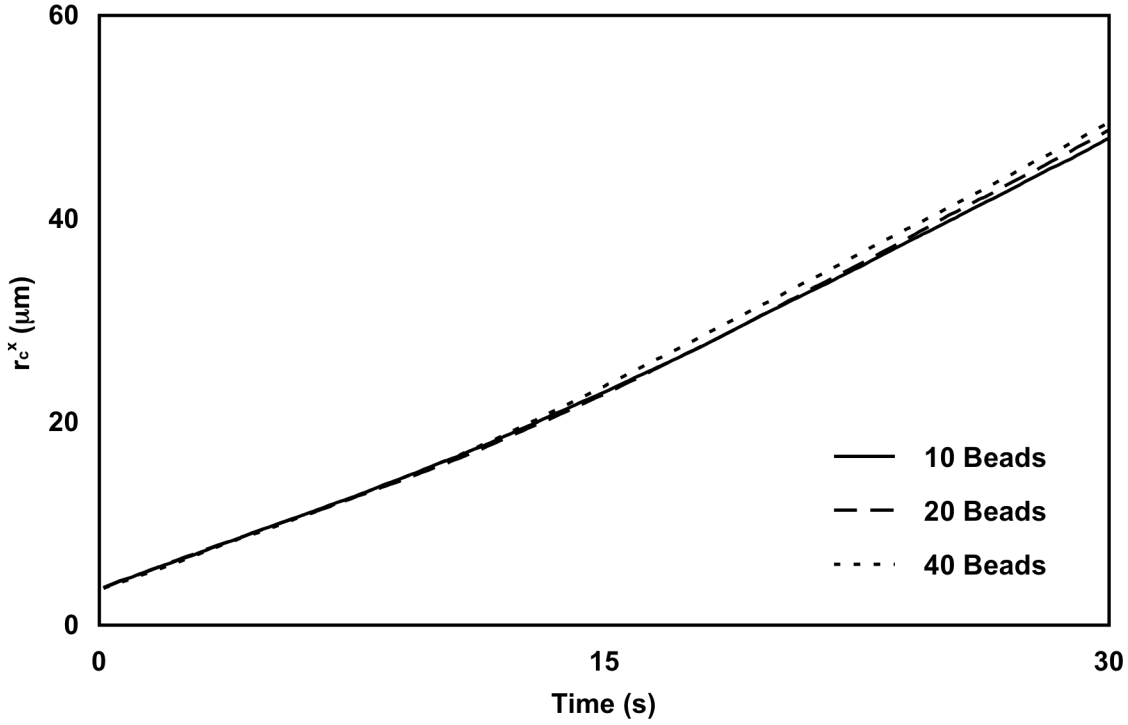

FIGURE 2.8 The same as figure 2.7 except this uses various numbers of beads.

It is important to note that we reach an upper limit in the achievable dimensionless velocity. We find that when we increase the non-dimensional fluid velocity we must also make a corresponding increase in the refinement to retain convergence with varying values of $\overline{A}$. We see that more beads are required for the same length chain, i.e. the length of each spring is shortened. The limit of more beads and shorter chains brings this analysis back into the (already explored) bead-rod region.

2.3 RESULTS

2.3.1 Definitions

We use our bead-spring simulations to model polymer chains of four different lengths. Three of these lengths are long enough that the number of Kuhn steps per spring is greater than 15 and therefore we use the WLC spring law for these long chains. These chains are 200μm (1515 Kuhn steps), 100μm (757 Kuhn steps), and 50μm (379 Kuhn steps) and they are all 20-bead simulations. We also consider two short chains – short enough that each spring is of length one Kuhn step. We use the FF spring law here because it gives a stiff rod-like spring. The short chains are 3.3μm (25 Kuhn steps) and 6.6 μm (50 Kuhn steps) and are 26-bead and 51-bead simulations. We first concentrate on the 100μm chain but we later expand our analysis to include the other lengths.

We evaluate our results using the steady state (or long time) ensemble-averaged collision distance ($\langle \Delta \bar{x} \rangle$) – this is the separation between where r_c^x *would be* if there were no obstacle (this is easily determined from the uniform velocity and time) and where r_c^x *actually is* after any entanglement interactions. Figure 2.9 is a graphical picture of how we determine $\langle \Delta \bar{x} \rangle$ in terms of length. This collision distance is made non-dimensional using the Kuhn step length. We also normalize this result using the number of Kuhn steps – this allows us to compare chains of different lengths. A large collision distance implies that the chain spent a large time interacting with the post. We choose this metric because it allows us easily to compare our results with the earlier of from Patel and Shaqfeh.[8]

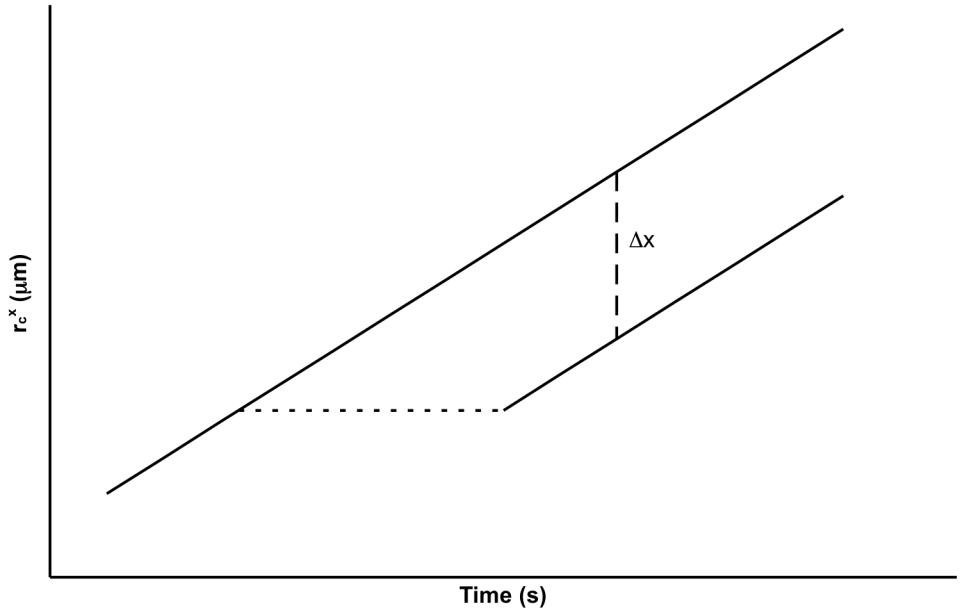

FIGURE 2.9 The collision distance (Δx) is the difference between where the polymer *would be* if there was no post and where the polymer *actually is* after any entanglement interactions.

The Peclet number represents the ratio of convective transport to diffusive transport. Patel and Shaqfeh[8] define Pe in with E as the electric field strength, λ as the charge per bead, and a as the Kuhn step length;

$$Pe = \frac{E\lambda\, a}{k_B T} \tag{2.17}$$

The mean bead velocity is related to the electric field by $V = E\lambda/\zeta_{Kuhn}$ where in the bead-rod model ζ_{Kuhn} is the bead drag coefficient. Substituting for $E\lambda$ in equation 2.17 gives

$$Pe_{Kuhn} = Pe = \frac{V\,\zeta_{Kuhn}\,a}{k_B T} \tag{2.18}$$

For our bead-spring model, we interpret ζ_{Kuhn} in equation 2.18 as the drag per Kuhn step which we obtain by dividing the total drag coefficient, ζ_{tot}, by the number of Kuhn steps, N_K, in the entire chain. The number of Kuhn steps in the entire chain is given by the ratio of the extended chain length to the Kuhn step length. This ensures that our value of Pe_{Kuhn} is physically equivalent to that of Patel and Shaqfeh and the results of our bead-spring simulations can be compared directly to the results of the bead-rod simulations of Patel and Shaqfeh. We call this Pe_{Kuhn} because it is based on the drag per Kuhn step. The drag per Kuhn step is the same for chains of different length. We also develop a second definition for the Peclet number.

$$Pe_{chain} = \frac{V\,\zeta_{tot}\,R_g}{k_B T} = Pe_{Kuhn}\left[\frac{\zeta_{tot}\,R_g}{\zeta_{Kuhn}\,a}\right] \tag{2.19}$$

Pe_{chain} is based on the total drag per chain and the radius of gyration. Longer chains experience greater drag, and this second definition allows us to more easily compare chains of different lengths.

2.3.2 X-offset and Y-offset

All of our simulation runs begin in the following manner. The polymer chain begins in a random coil orientation and it is set a small distance ahead of the obstacle. The right-most bead (the bead with the largest x-component) is placed at a distance 1/10 of R_g upstream of the post. For the 100μm chain one-tenth of R_g is equal to 1.12 Kuhn steps. Each trial uses a different initial configuration but the same upstream distance. One effect of the random coil configuration (rather than the 'extended line' that we used for the original convergence tests) is that the chain is now more likely to pass the post without any lasting interaction – it is possible for the chain to drift above or below the post without forming the interesting pulley effect. We see a decrease in average interaction time due to the fact that a percentage of the trials do not fully interact with the post.

We also vary the initial y-offset in some simulations using the 100μm chain. The y-offset (ε) is the distance (made non-dimensional by the Kuhn step) in the y-direction between the coil center-of-mass and the post. The coil is directly aligned with the post when the y-offset is equal to zero. We perform simulations (for the 100μm chain) over a wide range of Pe_{Kuhn} ($0.0001 \le Pe_{Kuhn} \le 0.0040$) with the same collection of initial y-offsets for each. Figure 2.10 shows the effect of increasing y-offset from zero to six. Each point on each curve is an average over 200 trials at that condition. Note that the collision distance is greatest at a y-offset of zero and that $\langle \Delta \bar{x} \rangle$ decreases as the y-offset is increased. The probability of forming a long-lasting pulley interaction is higher when the chain is directly aligned with the post – a y-offset of zero results in the highest

number of these interactions. Figure 2.10 shows the effect of increasing Pe_{Kuhn} for a number of initial y-offsets. We note that $\langle \Delta \bar{x} \rangle$ is greatest at the highest Pe_{Kuhn}. The polymer escapes the post interaction when one arm translates back against the flow and passes the post on the other side. It is more difficult for this to happen when the fluid velocity is high. We find that the collision distance is largest at highest Pe_{Kuhn} for any choice of y-offset.

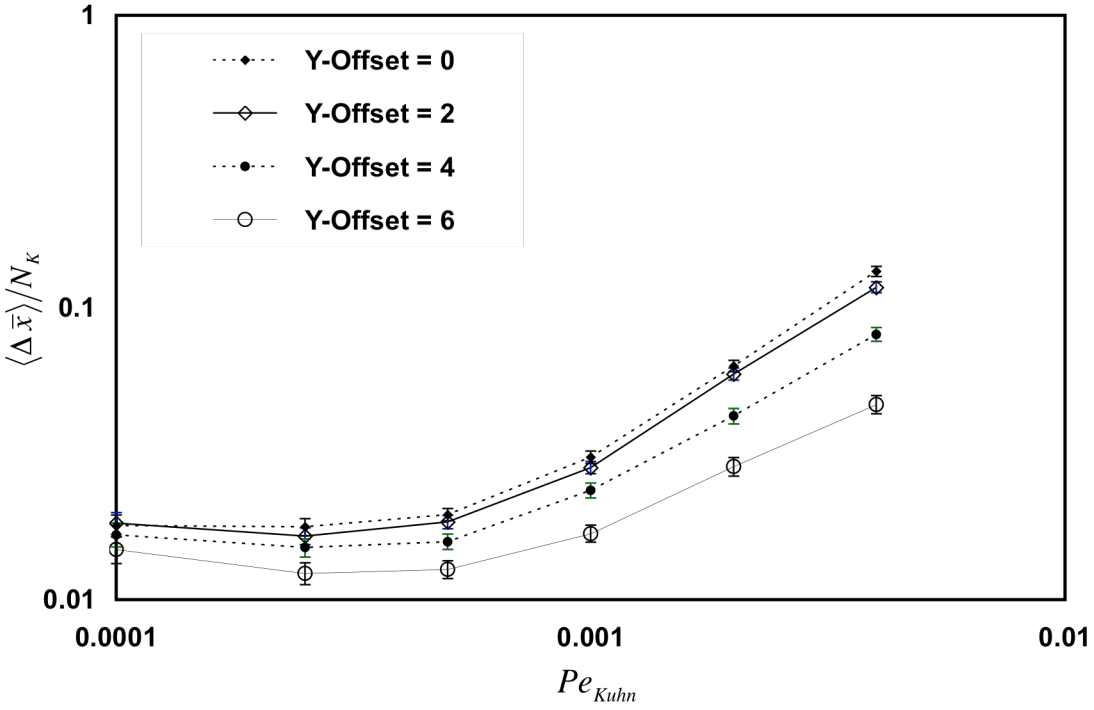

FIGURE 2.10 Ensemble-averaged collision distance ($\langle \Delta \bar{x} \rangle / N_K$) versus the Peclet number (Pe_{Kuhn}) for various values of y-offset.

We test the dependence on the initial starting position in the x-direction using the 100μm chain. This is the x-offset and it is made non-dimensional by the Kuhn step. This is a

measure of how far upstream the right-most bead is (how close is the coil to the post when the simulation begins). We selected four choices of x-offset all within about one Kuhn step of the post to see if the results are insensitive to the exact position of the coil upstream of the post, assuming "close" initial proximity (1.12 Kuhn steps is 1/10 of the radius of gyration). The x-offset was varied by more than 100-fold within this range and the result in x-displacement was the same within 10%. Thus we find that varying x-offset within this range has a negligible effect on our results, not only for zero y-offset but for non-zero y-offsets as well, and we maintain an x-offset of 1/10 R_g for all our simulations.

2.3.3 Collision Distance

We expand our analysis to include two additional chains of "long" length – 50μm (379 Kuhn steps) and 200μm (1515 Kuhn steps). We explore a wider range of Pe_{Kuhn} - varying from 0.0001 to 0.01 for these long chain simulations. We still have the limit that Pe_{Kuhn} cannot exceed 0.01 due to the demand for finer scale coarse graining but we are able to push well into the region of low Pe_{Kuhn}. We find in figure 2.11 that all three chains show a gentle increasing slope at relatively low Pe_{Kuhn} and switch to a more aggressively increasing slope at relatively high Pe_{Kuhn}. All three lengths nearly overlap in their gentle sloping portions. They switch to their steeply sloping portions as Pe_{Kuhn} is increased with the longest chain (1515 Kuhn steps) switching at the lowest Pe_{Kuhn} and the shortest chain (379 Kuhn steps) switching at the highest Pe_{Kuhn}. Each of the three lengths has a distinct aggressively sloping portion, but each of these three portions has a similar

slope. And these slopes are evenly spaced apart. Recall from earlier that we are limited to low Pe_{Kuhn} due to coarse graining concerns.

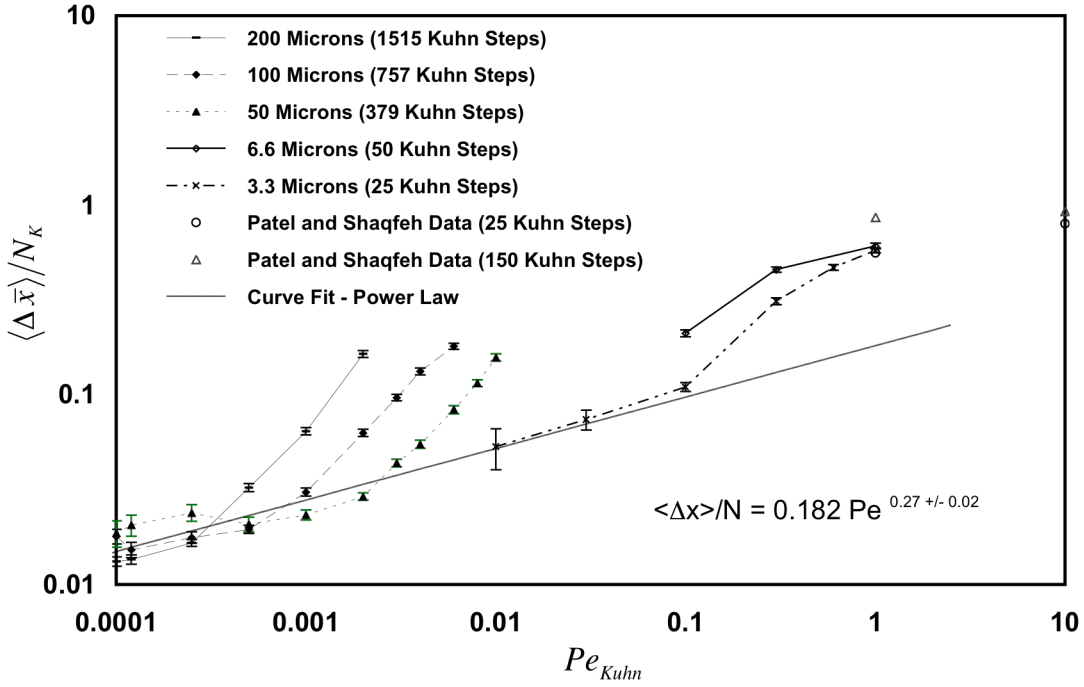

FIGURE 2.11 Ensemble-averaged collision distance ($\langle \Delta \bar{x} \rangle / N_K$) versus the Peclet number (Pe_{Kuhn}) for chains of various lengths. Also included is a power law curve fit and previous published results from Patel and Shaqfeh.

We are able to reach high values of Pe_{Kuhn} when we simulate much shorter chains. We model a short chain of 3.3μm (25 Kuhn steps) in a range of $0.01 \le Pe_{Kuhn} \le 1.0$ using the FENE-Fraenkel spring law to model each Kuhn step as a single stiff spring. This short chain shows a behavior very similar to that of the longer chains – it has a gentle sloping portion at relatively low Pe_{Kuhn} and a more aggressively increasing slope at relatively

high Pe_{Kuhn}. The short chain also shows a third region – there is the beginning of a leveling off at the highest Pe_{Kuhn} to a constant value of $\langle \Delta \bar{x} \rangle / N_K$. The slope of the gentle section is roughly parallel to the slope of the gentle section from the long chain simulations. A curve fit of the points in the gentle sloping region yields the following relationship.

$$\langle \Delta \bar{x} \rangle / N_K = 0.182 \, Pe_{Kuhn}^{\,0.27 \pm 0.02} \tag{2.20}$$

We include on figure 2.11 some results achieved earlier by Patel and Shaqfeh[8] using short bead-rod chains at high Pe_{Kuhn}. We note that our result for a 25-Kuhn-step chain at $Pe_{Kuhn} = 1.0$ agrees very well with their previously published findings. Notice that the 25-Kuhn-step data shows that $\langle \Delta \bar{x} \rangle / N_K$ for this chain approaches a constant upper limit at $Pe_{Kuhn} \approx 10.0$. Notice also that the 150-Kuhn-step data reach a similar upper limit at a lower Pe_{Kuhn}, around $Pe_{Kuhn} = 1.0$ or less. We believe that chains of all lengths will reach this constant value and that the Pe_{Kuhn} at which they reach it is a function of chain length. Notice that the data for the long chains (379 – 1515 Kuhn-steps) can be projected to reach this upper limit at $0.01 \le Pe_{Kuhn} \le 0.1$ (but we are unable to simulate the long chains in this region).

Figure 2.12 plots the same data against Pe_{chain} rather than Pe_{Kuhn}. Again we see that all lengths yield similarly shaped curves. They all have a similar transition from a shallow to a steep slope, and the slopes are similar for all lengths. For all chains, the change in slope occurs at the same value of $Pe_{chain} = 8.0$. The first three plots of Figure 2.13 were

generated by plotting the value of Pe_{chain} at which $\langle \Delta \bar{x} \rangle / N_K$ reaches a specified value, namely $\langle \Delta \bar{x} \rangle / N_K = 0.06$, $\langle \Delta \bar{x} \rangle / N_K = 0.10$, or $\langle \Delta \bar{x} \rangle / N_K = 0.14$, against chain length. We also find that the exponent for a power-law fit to these plots seems to be level off to a constant value around 0.50 as $\langle \Delta \bar{x} \rangle / N_K$ is increased.

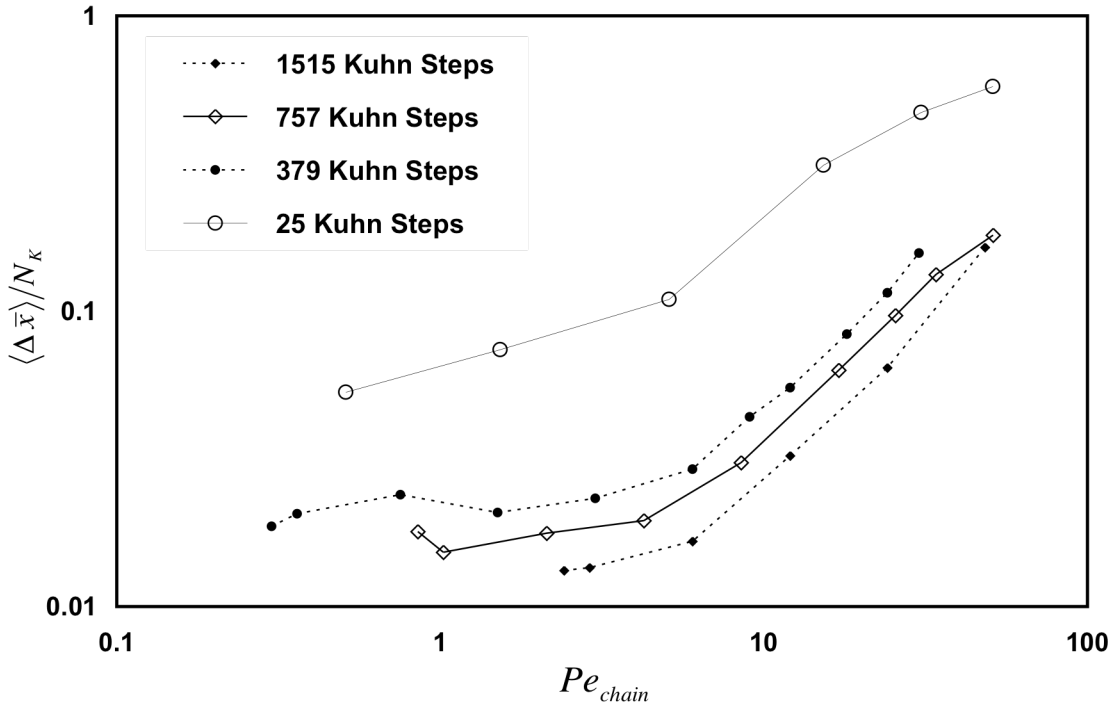

FIGURE 2.12 Ensemble-averaged collision distance ($\langle \Delta \bar{x} \rangle / N_K$) versus the re-scaled Peclet number (Pe_{chain}) for chains of various lengths. Notice the similar shaped curves.

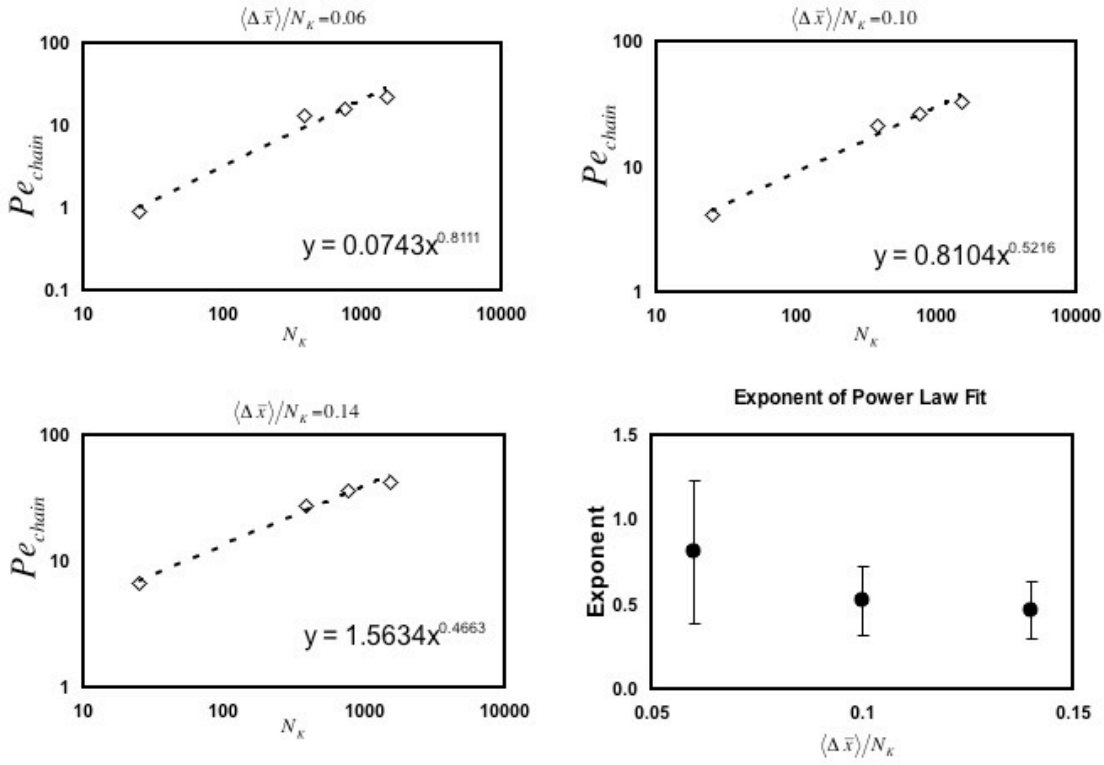

FIGURE 2.13 Power law curve fits for values of Pe_{chain} as a function of chain length for select choices of $\langle \Delta \bar{x} \rangle / N_K$. The exponent of the power law approaches 0.5 as $\langle \Delta \bar{x} \rangle / N_K$ increases.

2.4 FUTURE DIRECTIONS

The method described here for preventing springs from passing through obstacles can be used to solve problems that involve long polymers with dilute entanglements. To apply our method more generally, it will be important to develop an efficient method for

selecting the values of the strength and range parameters of the spring repulsion potential that produces results insensitive to their precise values. Here we found that a good choice of the range is a distance somewhat smaller than a Kuhn step and the optimal strength is probably related to the velocity of the fluid flow. The simulation requires finer coarse graining (the use of more beads) to achieve better resolution at higher velocities. At high velocities, one must represent each Kuhn step by a rod or stiff FENE-Fraenkel spring, and in this limit the greater efficiency of our method of imposing entanglement constraints relative to methods that impose excluded volume forces on the beads diminishes considerably.

2.5 SUMMARY

We have developed a bead-spring BD simulation that introduces a repulsive force between each spring and a topological obstacle where the repulsion decreases exponentially with separation distance. We have applied this to a long DNA polymer driven electrophoretically around an impenetrable post. This new method extends that of Kumar and Larson by allowing springs temporarily to pass through the post. Such "breaks" are kept track of and "repaired" in subsequent time steps through a potential that exponentially increases as the penetration of the "broken" spring beyond the post increases. Allowing these temporary "breaks" permits much larger time steps to be taken than can be allowed if the topological interactions were to be held inviolate through use of a very steep potential. The new method still satisfies the topological restrictions in a coarse-grained sense consistent with the coarse-graining already present in a bead-spring

model. To implement the method we determine the shortest distance of separation between each of the springs and the obstacle and distribute a repulsive force to each of the two beads at either end of the spring using the lever rule. We then check the spring for any crossings through the pole using a fast cross product method that misses no real breaks but reports some spurious breaks that are not real. We reject these few spurious breaks using a slow but rigorous "triangle method" developed by Kumar and Larson for definitely identifying breaks. The potential is then used to correct any broken springs in subsequent time steps. We test for convergence and robustness of our method to variations in the strength of the repulsive force, the range over which the repulsive force acts, the time step, and the number of beads used to model a 100 μm DNA polymer.

We measure the ensemble-averaged collision delay distance ($\langle \Delta \bar{x} \rangle$) to quantify the results of our tests. Our data are consistent with, and extend, previously published results found using bead-rod simulation of shorter polymer chains at higher effective fields. We include our results (1515, 757, 379, and 25 Kuhn-steps) with those from short bead-rod chains (25 and 150 Kuhn-steps) studied by Patel and Shaqfeh on a rescaled plot. Our method is able to simulate arbitrarily long chains at low electrophoretic velocities. This complements the bead-rod method that cannot access low velocities for very long chains because of the small time step intrinsic to bead-rod methods. A plot of $\langle \Delta \bar{x} \rangle / N_K$ vs. Pe_{Kuhn} shows three regimes: a high fluid velocity regime – $Pe_{Kuhn} \geq 1.0$ (which is captured by using bead-rod or bead-FF spring simulations of short chains) – in which $\langle \Delta \bar{x} \rangle / N_K$ is independent of Pe_{Kuhn}, an intermediate regime in which

$\langle \Delta \bar{x} \rangle / N_K^{1/2} \propto Pe_{chain}$, and a low fluid velocity regime – $Pe_{chain} \leq 8.0$ – in which $\langle \Delta \bar{x} \rangle / N_K \propto Pe_{Kuhn}^{0.27 \pm 0.02}$.

REFERENCES

[1] de Carmejane, O.; Yamaguchi, Y.; Todorov, T.I.; Morris, M.D. *Electrophoresis* **2001**, *22*, 2433.

[2] Barron, A.E.; Soane, D.S.; Blanch, H.W. *Journal of Chromatography A* **1993**, *652*, 3.

[3] Doyle, P.S.; Bibette, J.; Bancaud, A,; Viovy, J.L. *Science* **2002**, *295*, 2237.

[4] Volkmuth, W.D.; Austin, R.H. *Nature* **1992**, *358*, 600.

[5] Volkmuth, W.D.; Duke, T.; Wu, M.C.; Austin, R.H. *Physical Review Letters* **1994**, *72*, 2117.

[6] Starkweather, M.E.; Muthukumar, M.; Hoagland, D.A. *Macromolecules* **1998**, *31*, 5495.

[7] Nixon, G.I.; Slater, G.W. *Physics Review E* **1994**, *50*, 5033.

[8] Patel, P.D.; Shaqfeh, E.S.G. *Journal of Chemical Physics* **2003**, *118*, 2941.

[9] Kumar, S.; Larson, R.G. *Journal of Chemical Physics* **2001**. *114*, 6937.

[10] Chopra, M.; Larson, R.G. *Journal of Rheology* **2002**, *46*, 831.

[11] Grassia, P.; Hinch, E.J. *Journal of Fluid Mechanics* **1996**, *308*, 255.

[12] Marko, J.F.; Siggia, E.D. *Macromolecules* **1995**, *28*, 8759.

[13] Somasi, M; Khomami, B.; Woo, N.J.; Hur, J.S.; Shaqfeh, E.S.G. *Journal of Non-Newtonian Fluid Mechanics* **2002**, *108*, 227.

[14] Sevick, E.M.; Williams, D.R.M. *Physical Review Letters* **1996**, *76(14)*, 2595.

[15] Padding, J.T.; Briels, W.J. *Journal of Chemical Physics* **2002**, *117*, 925.

[16] Hsieh, C.; Jain, S.; Larson, R.G. *Journal of Chemical Physics* **2006**, *124*, 044911.

[17] Saville, P.M.; Sevick, E.M. *Macromolecules* **1999**, *32*, 892.

[18] Randall, G.C.; Doyle, P.S. *Physical Review Letters* **2004**, *93*, 058102.

CHAPTER 3

MULTIPLE REGIMES OF COLLISION OF AN ELECTROPHORETICALLY TRANSLATING POLYMER CHAIN AGAINST A THIN POST

We use a previously developed bead-spring Brownian dynamics model for simulating the topological interactions between polymers and thin obstacles to study electrophoretically translating DNA strands interacting with an immovable post over a wide range of chain lengths ($25 \le N_K \le 1500$) and field strengths or velocities ($10^{-4} \le Pe_{Kuhn} \le 10^{0}$). Here N_K is the number of Kuhn steps in the chain and Pe_{Kuhn} is the Peclet number based on the Kuhn length. This Peclet number is the ratio of the field-induced polymer motion to the Brownian motion. We find that the mean distance $\langle \Delta \bar{x} \rangle$ that the chain migration is held up by the entanglement interaction increases with higher fields, encompassing four distinct regimes. The two fastest regimes exhibit the classic rope-and-pulley dynamics, in which the chain is draped around the entanglement and the longer of the two dangling ends pulls the shorter end around the obstacle. In one of these regimes, occurring at the highest field strength, the dimensionless delay distance reaches its theoretical upper limit at $\langle \Delta \bar{x} \rangle / N_K = 0.5$ and in the other, at moderately high field strength, the ends of the chain remain balled up while the central portion is extended, creating a "ball and chain" configuration. In the two slower regimes, the polymer retains a coil-like shape as it

diffuses laterally and eventually clears the post without deforming. We develop models that describe both the average delay and the distribution of delays for all regimes, except the slowest one, which is distinguished by a peculiar fractional power law relationship $\langle \Delta \bar{x} \rangle / N_K \propto Pe_{Kuhn}^{0.27}$.

3.1 INTRODUCTION

Long polymer chains, such as DNA, can be separated by length by driving them electrophoretically through a mesh of obstacles, such as a polymer gel matrix, or a microfabricated array of posts[1,2,3,4]. In all such processes, the basic interaction that leads to a polymer-length-dependent delay is an entanglement of the polymer with the post. Hence there is considerable interest in understanding how this delay is produced and in modeling its dependence on chain length and field strength. The simplest model that allows the basic entanglement interaction to be studied with the fewest distracting complications is that of a single long polymer molecule encountering a single thin post. This case has been studied, experimentally[5,6], computationally[7,8,9,10,11], and theoretically[12], but almost all studies have focused on the "high field" regime in which the polymer, when encountering the post, forms a "rope-and-pulley" structure with two extended arms, one on either side of the obstacle, and the interaction is governed by the rate in which the shorter of the two arms is pulled back and around the post by the force exerted on the longer arm. Cases of lower field strength have not been much studied.

Simulations reported in the literature use models such as the pearl necklace and the bead-rod models, which are simulated with Brownian dynamics or Monte Carlo simulations. These models are limited to rather short chain lengths and fast electrophoretic velocities because they are coarse-grained at the level of a Kuhn step length (which is the length of a rod in a bead-rod simulation and can be thought of as the effective random-walk step size of the polymer chain). Many 100's or 1000's of rods would therefore be required to simulate a long polymer using a bead-rod simulation, which is computationally overwhelming. To overcome this, we have developed a bead-spring model in which each spring can represent many Kuhn steps and yet preserve topological "non-crossability" constraints and so we are able to evaluate longer chains in slower fields than has been previously possible. In work reported elsewhere[13] we showed that, with our new Brownian dynamic method with spring non-crossability, we could span an unlimited range of chain lengths, exemplified by simulating chains with lengths in the range $25 \le N_K \le 1500$ (N_K is the number of Kuhn steps in the chain), and a wide range of field strengths, covering the range $10^{-4} \le Pe_{Kuhn} \le 10^{0}$ in example simulations (Pe_{Kuhn} is the Peclet number based on the Kuhn step length which we will define more precisely shortly).

Figure 3.1 shows our previous findings, as well as two data points from a previously published bead-rod simulation from another group[10]. Here we propose that the interactions between the chain and the thin post can be grouped into four distinct regions (see figure 3.1), distinguished by the field strength and chain length, and we develop predictive models for the physics of all of the regions, except the slowest region – Region

1 – which we explain only qualitatively. We have explicit simulation data in the two regions of lowest field strength (R1 and R2); we borrow from the literature to describe the region in the highest field strength (R4); and we will develop an approximation to predict the data in the transition region (R3) between R2 and R4.

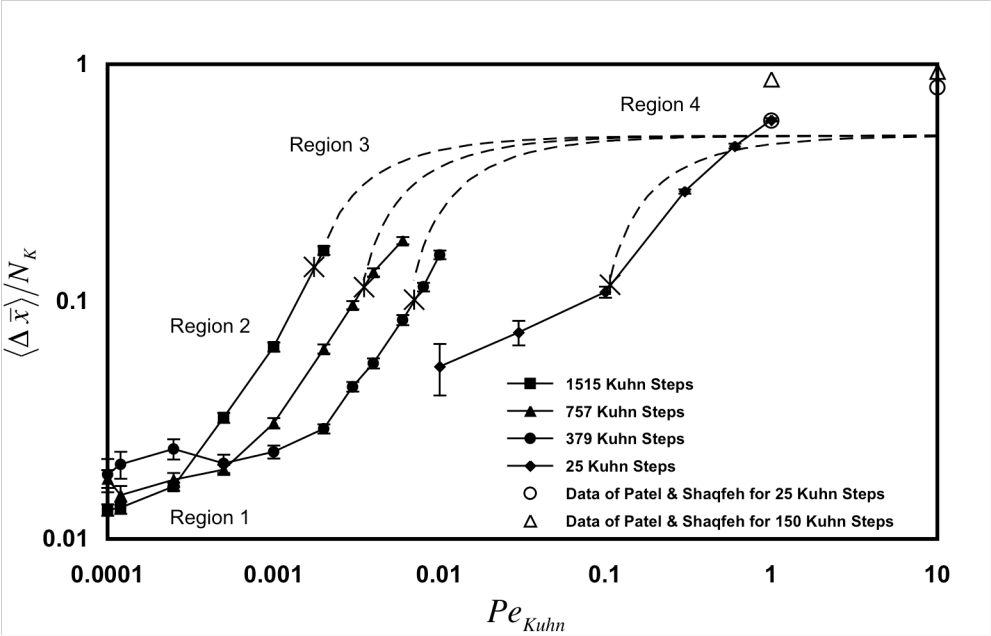

FIGURE 3.1 Master plot of normalized delay distances $\langle \Delta \bar{x} \rangle / N_K$ as functions of Pe_{Kuhn} for chains of four different lengths. The results for the three longest length chains (N_K = 379, 757, and 1515) were obtained using coarse-grained bead-spring simulations in which each spring represents many Kuhn steps, while for the shortest chain (N_K = 25), 25 stiff Fraenkel springs were used, which resembled rods. The dashed lines represent the theoretical predictions for Region 3 for each of the four chain lengths. The Patel and Shaqfeh data are for bead-rod simulations at high Pe_{Kuhn}. The large asterisks show the values of Pe_{Kuhn} where σ^2/μ^2 transitions from Region 2 into Region 3, as shown in figure 3.10.

We measure the effect of the interaction between the chain and the post using the steady state ensemble-averaged collision delay distance ($\langle \Delta \bar{x} \rangle$). This measure has been made non-dimensional by division by the Kuhn step length (b_K). $\Delta \bar{x}$ is the dimensionless difference between the x-location (where x is the field direction) of the center of mass of a chain in a simulation containing the obstacle and one translating at the average speed the chain would move without the obstacle. The location of the center of mass of a chain without the obstacle is easily calculated from the known uniform velocity and the elapsed time. A positive $\Delta \bar{x}$ represents a distance penalty that the chain suffers as a result of its entanglement interaction. A large collision distance implies that the chain is greatly delayed by the post. We normalize this measure by N_K, the number of Kuhn steps in the chain. (We note that to relate our results to those of fine-scale bead-rod models, we use N_K to characterize chain length even though our simulations are carried out with a coarse-grained bead-spring model in which each spring represents $N_{K,s} = N_K / N_S$ Kuhn steps, where N_S is the number of springs used to represent the entire molecule.)

Randall and Doyle[6] have determined experimentally and theoretically the value of 0.5 for the upper limit of $\langle \Delta \bar{x} \rangle / N_K$ in R4. We will explain our approximation method for R3 in the discussion section of this work. We will also describe the physics that govern the dynamics in R2 and R3. We suggest a possible mechanism dominating R1 but without making quantitative predictions for this regime.

3.2 METHODS

We detailed in a previous chapter a method that allows us to impart spring-post repulsions into Brownian dynamics bead-spring simulations of arbitrarily long chains. This method reaches convergence with respect to changes in the time step (Δt), the number of springs (N_S), and the parameters used in the repulsive spring potential (namely the range and strength of the potential[13]), so that the predictions are free of dependence on these non-physical simulation parameters, and should be virtually identical to those that would be obtained from a fine-grained bead-rod model.

Our method is restricted in that the minimum number of springs necessary to achieve convergence is a function of the field strength (Pe_{Kuhn}) because the configurations become more distorted at higher fields and they require more and shorter springs to resolve the tight bends produced in the chain at high fields. There is thus a limit to how large a field strength we can simulate for each chain length, a limit that is set by the computational resources available. Moreover, our method provides no advantage over simpler bead-rod simulations if the number of springs we require to achieve convergence approaches the number of Kuhn steps in the chain. This limit is approached at high fields. Hence, we are able to simulate long chains at low Pe_{Kuhn} using the coarse-grained bead-spring model and short chains at high Pe_{Kuhn} using a fine-grained bead-Fraenkel-spring model in which each spring is effectively a rod, but not long chains at high Pe_{Kuhn}. This is why some parts of figure 3.1 are missing and will be filled in with predictions that we will describe below.

Note that the Peclet number is a ratio between the rates of electrophoretic transport and diffusive transport. A high Peclet number implies that the drag dominates while a low Peclet number implies that the Brownian motion is dominant. We define a microscopic Peclet number that balances convection and diffusion at the level of a Kuhn step length as:

$$Pe_{Kuhn} = \frac{V \zeta_{Kuhn} b_K}{k_B T} \tag{3.1}$$

where V is the velocity of the coil in the absence of the post and is directly proportional to the field strength. For our bead-spring model, we interpret ζ_{Kuhn} in equation 3.1 as the drag per Kuhn step, $\zeta_{Kuhn} \equiv \zeta_{tot} / N_K$, which we obtain from the total drag coefficient summed over all beads, $\zeta_{tot} \equiv \zeta_b (N_s + 1)$, where ζ_b is the bead drag coefficient divided by the number of Kuhn steps, N_K, in the entire chain. The number of Kuhn steps in the entire chain is given by the ratio of the extended chain length to the Kuhn step length. We take ζ_{Kuhn} to be the same for chains of all lengths. Longer chains therefore have a higher total drag and also have correspondingly more Kuhn steps.

We model polymer chains of four different lengths: 1515 Kuhn steps (200 μm), 757 Kuhn steps (100 μm), 379 Kuhn steps (50 μm), and 25 Kuhn steps (3.3 μm). The lengths in the parentheses are the approximate lengths of double-stranded DNA molecules having the corresponding numbers of Kuhn steps. We take the Kuhn step length to be $b_K = 0.132\ \mu m$, corresponding to that for optically stained double-stranded DNA

molecules[14]. The three longer chains are modeled with 20-bead simulations and we use the worm-like chain spring law because the number of Kuhn steps per spring is greater than 15. The shorter chain is modeled with a 26-bead simulation and for it we use the "FENE-Fraenkel" spring law because it results in a stiff rod-like spring, and thus these chains mimic bead-rod chains, which are appropriate, and are computationally tractable, for shorter chains[13,15].

Each simulation begins with a random coil (each run has an independent random coil configuration) that is initially placed a small distance upstream (to the left) of the post (with the downstream-most bead of the coil a distance of $0.1R_g$ away from the post and the results are insensitive to exactly how close this is). The coil is also placed such that its center of mass is in line with the center of the post. A drag force equal to $\zeta_b V$ is imposed on each bead of the chain to drive it downfield. The simulation continues until the last bead to pass the post (the leftmost bead) reaches a distance of more than seven-and-a-half Kuhn lengths downstream of the post, which is far enough to be sure that it is no longer entangled with the post. The time t required to reach this position is then converted into a delay distance Δx by subtracting the distance traveled (the difference between the original location of the center of mass and the location of the center of mass at the end of the run), from the distance Vt a chain would have traveled in the same time t in the absence of the post and without diffusion. The value Δx is made dimensionless, $\Delta \bar{x} \equiv \Delta x / b_K$, as described above. Each data point in figure 3.1, representing a single chain length and value of Pe_{Kuhn}, is the mean normalized delay distance $\langle \Delta \bar{x} \rangle / N_K$ averaged over 800 trials (although some data points are averaged over 3200 trials – this is

discussed later). Further details of the simulation can be found in Holleran and Larson[13].

The measure of the strength of interaction between the chain and the post is $\Delta \bar{x}$ – the distance penalty associated with the entanglement. There is a higher penalty at higher "flow rates" because the chain *would have* moved farther downstream in a given period of time if there had been no post.

3.3 RESULTS AND DISCUSSION

3.3.1 Region 4 (R4)

Convective transport is the dominant driving force in Region 4 (R4). It is in this region where the rope-and-pulley formation is most prevalent. This has been discussed elsewhere by Randall and Doyle[6] and Patel and Shaqfeh[10]. Randall and Doyle state that at high enough Pe_{Kuhn} chains of all lengths will reach an asymptotic delay $\langle \Delta \bar{x} \rangle / N_K = 0.5$ and this result will be independent of Pe_{Kuhn} above a critical value of Pe_{Kuhn}. Our results indicate that longer chains enter R4 at lower values of Pe_{Kuhn} (see figure 3.1).

All chains in R4 form the rope-and-pulley interaction because the convective force is too great to allow diffusion to help move the chain around the post. The random Brownian motions have a negligible effect at this Pe_{Kuhn}. The coil usually forms two extended arms (one on either side of the post) and escape is controlled by how long it takes for the

shorter arm to be pulled back (by the spring force) around the post. One key variable is the location along the length of the chain where the intersection with the post will occur (the location of the pulley). For a collection of truly random collisions the length of the shorter arm is evenly distributed between zero and one-half of the total length of the chain. The longest entanglement interaction thus occurs when the polymer intersects the post at a location near the midpoint of the chain.

We attempted to reach R4 with our simulations, but we run up against the limitation that an increase in Pe_{Kuhn} requires an increase in the number of springs needed to obtain converged results that are insensitive to the number of springs used. We came closest to reaching R4 for our work with the shortest chain at high field strengths. Recall that the each data point on figure 3.1 is an average over 800 trials. Even though we do not reach a high enough Pe_{Kuhn} to find a regime where $\langle \Delta \bar{x} \rangle$ is independent of Pe_{Kuhn}, we are able to see some individual trials that clearly show the rope-and-pulley dynamics. Figure 3.2 contains frames from a movie of the 25 Kuhn step chain at $Pe_{Kuhn} = 1$. It is clear in this series of images that the chain has formed two separate and distinct arms.

We must note that we actually find a case where $\langle \Delta \bar{x} \rangle > 0.5$ – this appears to contradict the theory of Randall and Doyle[6]. We can explain this by noting that there is a bias in our set-up – we are unfairly favoring longer lasting interactions at high Pe_{Kuhn} because we begin with the chain lined up with the post and therefore with a somewhat greater likelihood of forming the collision near the center of the chain than near the ends. This is a negligible effect at low Pe_{Kuhn} because there is ample opportunity for the diffusion to

eliminate the bias, but at high Pe_{Kuhn}, where convection dominates diffusion, this effect can produce an increase in long-lasting interactions.

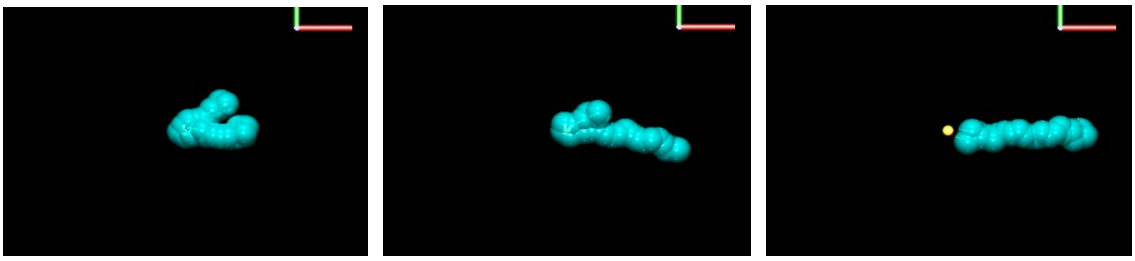

FIGURE 3.2 Images from simulations of polymers escaping from entanglements with a post, where the post is shown by a dot. This shows a 25-Kuhn-step chain under strong flow ($Pe_{Kuhn} = 1$). The rope-and-pulley formation (common for Region 3 and Region 4) is evident. The "camera" (or view) is in close in because this is a short chain.

We evaluated the effect of the bias that led to too many long-time interactions and resulted in $\langle \Delta \bar{x} \rangle > 0.5$, by re-running the simulations for the two highest Pe_{Kuhn} with the initial location of the center of the coil varying laterally uniformly over the range $\pm R_g$ away from a head-on impact with the post. This allowed some chains that were not lined up with the post to simply brush past the post without having a rope-and-pulley interaction. With this distribution of initial positions, we found that $\langle \Delta \bar{x} \rangle$ dropped by a factor of two for both $Pe_{Kuhn} = 0.60$ and $Pe_{Kuhn} = 1.00$ and fell well below the $\langle \Delta \bar{x} \rangle = 0.5$ limit from Randall and Doyle. We note that the points from Shaqfeh and Patel (on figure 3.1) are also above the $\langle \Delta \bar{x} \rangle = 0.5$ limit by roughly a factor of two, presumably because their chains were also lined up exactly with the post, with no offset, as ours were. We

believe that if Shaqfeh and Patel had removed their bias in the location of chain-post, their results would also have been beneath the limit.

Randall and Doyle relate the time required for the chain to unhook from the post to the location along the chain where the interaction begins. Thus, in R4, they showed that[6]

$$t_{unhook} = -\frac{L}{2\mu E}\ln\left(1-\frac{2x_1}{L}\right) \tag{3.2}$$

Where L is the length of the chain, x_1 is the length of the shorter arm, and μE (the product of mobility and field strength) is the polymer velocity V created by the electric field. We can recast this equation to measure dimensionless delay distance so that it corresponds with our method of analysis. We first define

$$y \equiv \frac{x_1}{L} \tag{3.3}$$

And we note that

$$\frac{\Delta \bar{x}}{N_K} = \frac{t_{unhook}}{(L/\mu E)} \tag{3.4}$$

And then we rewrite equation 3.2 for R4

$$\frac{\Delta \bar{x}}{N_K} = -\frac{1}{2}\ln\left(1-2y\right) \tag{3.5}$$

This has the appropriate behavior. The distance penalty is zero when $y = 0$ – this is the case when the interaction occurs at the endpoint of the chain. The distance penalty is infinitely large when $y = 0.50$ – this is the case when the interaction occurs at the exact center of the chain.

3.3.2 Region 3 (R3)

Region 3 (R3) is similar to R4 in that the chain still forms the classic rope-and-pulley configuration. However, in this region, the convective force is not strong enough to fully uncoil the ends of the two arms. The chain is *mostly* fully stretched expect at the ends of the arms where some of the monomers exist in the form of a coil or clump. The size of the clump (i.e. the number of monomers in the clump) is a function of Pe_{Kuhn} – as the field strength is lowered more monomers, and a greater fraction of the chain length, (more of the chain length) are found in the end coils. There is still sufficient force for part of the chain to be fully extended but not enough for the ends, which have the least tension, to be fully extended. The fraction of chain in the coils (material which is not contributing significantly to the length of the arms) is inversely related to the field strength. We use a simplified idea to model this. We imagine the central part of the chain to be fully extended with a ball of monomers at each end, where the size of the ball depends on the Peclet number.

This "ball and chain" concept will reduce the $\langle \Delta \bar{x} \rangle$ values in this region for two reasons. First, there is a shorter length of chain that needs to be pulled back around the pulley. Imagine a scenario in which the chain intersects the post in such a way that 35% of the chain is in the shorter arm ($y = 0.35$). In R4 the length of chain that must be pulled back is equal to 35% of a fully extended chain. In R3 the length of chain that must be pulled back is less because some of the length is in the ball and *not* fully extended – this will result in a quicker escape. In addition, in R3, there are some cases when the interaction will have a zero delay because the intersection point is *inside* of the ball – this chain will get past the post without any delay.

We define b as the fraction of the chain in each ball. The dimensionless length of the short arm (y) can vary between zero and one-half (as was discussed in R4); thus b is also allowed to vary between zero and one-half. We have $b = 0$ when the short arm is fully extended (case R4) and $b = y$ when the entire amount of the shorter arm is in the end coil (and this case will result in a zero time interaction).

Now consider our data for the 25 Kuhn step chain – this is the only length chain that we were able to simulate at a high enough Pe_{Kuhn} to obtain data in the R3 range. For a chain with only 25 Kuhn steps there are rather few monomers available to distribute between the extended and coiled portions of the chain. The ball and chain idea should work much better for the longer chains because for them it is easier to have a sizable number of monomers in *both* the ball and chain portions. However, we have no simulation data in

R3 for long chains and we must content ourselves with testing the ball and chain model using the results for the 25 Kuhn step chain.

We show in figure 3.3 histograms for all of the $\Delta \bar{x}/N_K$ values for the 25 Kuhn step chain. There are six curves here – one for each of the six Pe_{Kuhn}. The peak of each curve shows the most common value for $\Delta \bar{x}/N_K$ at that Pe_{Kuhn}. Notice that, starting from the lowest value of Pe_{Kuhn}, the peak initially moves to the right as Pe_{Kuhn} is increased. However, for $Pe_{Kuhn} \geq 0.10$, the peak remains at the same $\Delta \bar{x}/N_K$ but begins to decrease in height. The contribution of the right-side tail becomes more significant at high Pe_{Kuhn}. The peak location remains at $\Delta \bar{x}/N_K = 0.2$ for $Pe_{Kuhn} \geq 0.10$, but, with increasing Pe_{Kuhn}, there are more long-lasting interactions. These long-lasting interactions lead to an increasing $\langle \Delta \bar{x} \rangle / N_K$ with increasing Pe_{Kuhn} up until a saturation point, which is expected when Pe_{Kuhn} reaches unity and R4 is entered. We note here that the curves for the three highest Pe_{Kuhn} are based on 3200 trials (while the curves for the three lowest Pe_{Kuhn} are based on 800 trials) – this was done to improve the statistics for our future analysis of the high Pe_{Kuhn} results.

We now return to the analytical result from Randall and Doyle that relates the delay distance to the location of the chain-post interaction. We can make an adjustment to this analysis to introduce our idea of the ball-and-chain effect in R3. We add a term to equation 3.5 to account for the fact that only the portion ($y - b$) of the short arm needs to be pulled over the pulley before the chain is released. For the purpose of this simplified analysis, the ball is assumed to be of essentially zero size and to roll instantaneously over

the pulley. However, we still assume that the ball exerts the same drag as it would if it were fully extended. Thus, we are here neglecting conformation-dependent hydrodynamic interactions and essentially assuming a free-draining chain, as is also assumed in our simulations. The delay induced by the last fraction *b* of the chain must therefore be subtracted from equation 3.5. This delay is $-1/2\ln(1-2b)$, which when subtracted from the right side of equation 3.5 gives

$$\frac{\Delta \bar{x}}{N_K} = -\frac{1}{2}\ln(1-2y) + \frac{1}{2}\ln(1-2b) \tag{3.6}$$

This extra term allows us to adjust $\Delta \bar{x}/N_K$ for various ball sizes. When $b = 0$, equation 3.6 reduces to equation 3.5 which is valid in R4.

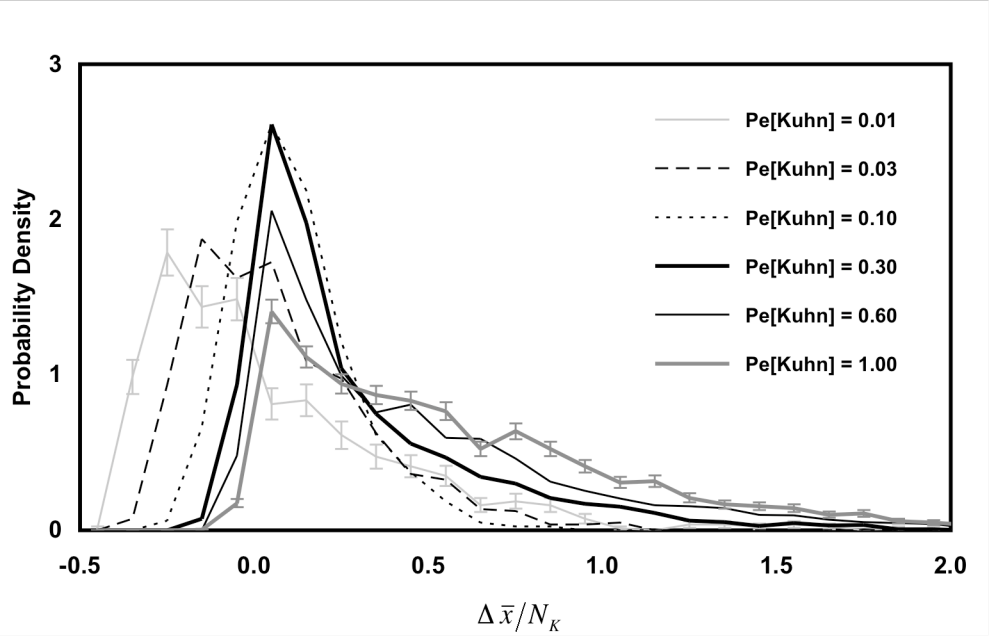

FIGURE 3.3 Probability distribution of $\Delta \bar{x}/N_K$ for various values of Pe_{Kuhn} for simulations of 25-Kuhn-step chains. Notice that at $Pe_{Kuhn} = 0.10$ there is a significant change in the shape of the curves. Typical error bars are shown for the highest and lowest field strengths.

We use this expression for the distribution of delay distances to find the probability distribution for $\Delta\bar{x}/N_K$ assuming that y is evenly distributed between zero and one-half. A delta function at zero is introduced to represent the cases in which there is a zero-delay interaction because the intersection point is located within the ball. The factor of two in the second term below is required so that the integral of the probability will sum to unity even in the case when $b = 0$:

$$P\left(\frac{\Delta\bar{x}}{N_K}\right) = 2b\,\delta(0) + 2(1-2b)\exp\left(-2\frac{\Delta\bar{x}}{N_K}\right) \tag{3.7}$$

We note that when $Pe_{Kuhn} = 1$ the ball should be fully unraveled because the drag induced by the field matches the Brownian force on a single Kuhn step. The end monomers begin to ball up for smaller Pe_{Kuhn} because there is then not enough drag force on the end Kuhn segment to overwhelm the Brownian force. However, for Pe_{Kuhn} slightly below unity, the drag force on the final few Kuhn segments will accumulate, producing enough tension to fully extend all but the last few Kuhn steps which form the "ball" at the end of the chain. Since, in the free-draining limit, the drag on the "ball" is proportional to the number of Kuhn segments in the ball, the number of Kuhn steps in the ball should be inversely proportional to Pe_{Kuhn}. Since b is the fraction of the Kuhn steps in the ball, we must have

$$b \approx \frac{1}{(Pe_{Kuhn}\,N_K)} \tag{3.8}$$

We are now able to use equations 3.7 and 3.8 to predict the probability distribution of $\Delta\bar{x}/N_K$ as a function of Pe_{Kuhn} in R3. Figures 3.4a, 3.4b, and 3.4c show our predictions and our simulation data for the three values of Pe_{Kuhn} that are in R3 for the 25 Kuhn-step chain. We evidently do a good job of predicting the tail portion of the distribution. There is some discrepancy at small $\Delta\bar{x}/N_K$ where our simple ball-and-chain model assumes that there is a delta function at $\Delta\bar{x}/N_K = 0$ corresponding to cases where the "ball" makes contact with the post and immediately escapes with zero delay. Obviously, in the simulations, these cases require a small but finite delay, and thus produce a peak at small $\Delta\bar{x}/N_K$ that is not captured in our over-simplified model.

We have no Region 3 data from the three longer chains to compare with theory. However, we can predict how these chains would behave in R3 by averaging over the probability distribution in equation 3.7:

$$\frac{\langle\Delta\bar{x}\rangle}{N_K} = \int_0^\infty P\left(\frac{\Delta\bar{x}}{N_K}\right)\left(\frac{\Delta\bar{x}}{N_K}\right) d\left(\frac{\Delta\bar{x}}{N_K}\right) \tag{3.9}$$

which, after a little mathematics, yields

$$\frac{\langle\Delta\bar{x}\rangle}{N_K} = \frac{1}{2}(1-2b) = \frac{1}{2}\left(1 - \frac{2}{Pe_{Kuhn}\, N_K}\right) \tag{3.10}$$

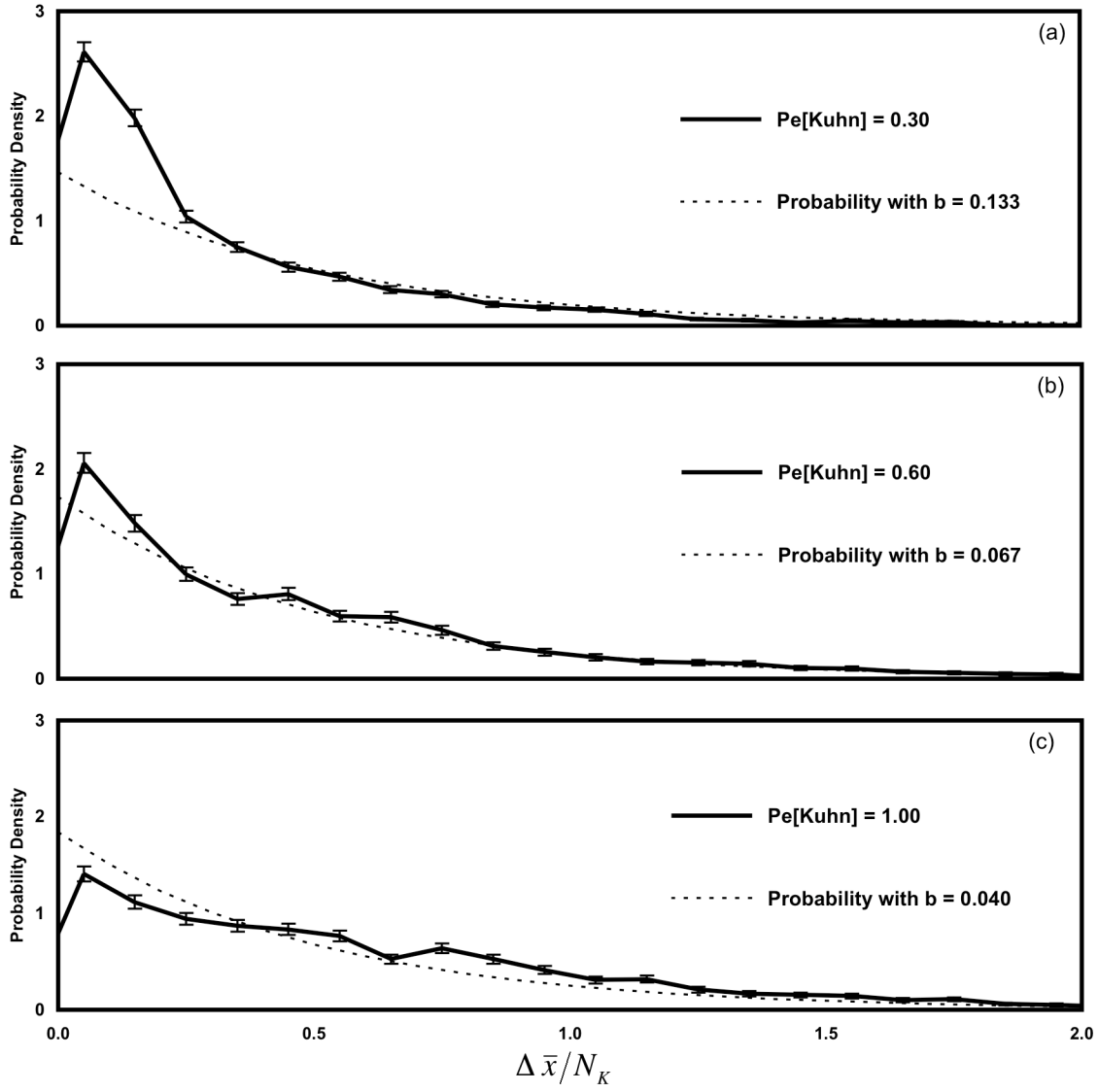

FIGURE 3.4 The solid line shows the probability distribution for the 25-Kuhn-step chain obtained from the simulation. The dashed line shows the prediction of the probability distribution with b given by equation 3.7, $b = 1/\left(Pe_{Kuhn}\, N_K\right)$. (a) $Pe_{Kuhn} = 0.30$ and $b = 0.133$. (b) $Pe_{Kuhn} = 0.60$ and $b = 0.067$. (c) $Pe_{Kuhn} = 1$ and $b = 0.04$.

Since figures 3.4a, 3.4b, and 3.4c show that our probability prediction is in good agreement with the limited delay distribution data we were able to acquire for R3 for the shortest chain, we feel confident in using this probability distribution to predict the curves of $\langle \Delta \bar{x} \rangle / N_K$ vs. Pe_{Kuhn} in R3 for chains of any length. Such predictions for chains of length 1515, 757, and 379 Kuhn steps are shown as dashed lines in figure 3.1. We calculate the curves down to the regions where they come into near overlap with the corresponding data that we have for these long chains. The reasonable match up of the curves predicted for R3 with the high Pe_{Kuhn} end of the R2 data for the long chains indicates that our theory for R3 is at least consistent with R2 simulation data. Note also that the predicted result in R3 for the shortest chain (25 Kuhn steps) is in reasonable agreement with data for this chain length, especially considering that the "ball-and-chain" model is not expected to work very well when the ball and the chain each contain only a few Kuhn segments, and so there is really no sharp distinction between the "ball" and the "chain". We also notice that equation 3.10 reaches Doyle-Randall limit of $\langle \Delta \bar{x} \rangle / N_K = 0.5$ as the field strength is increased (in the limit of high Pe_{Kuhn}).

3.3.3 Region 2 (R2)

In Region 2 (R2) the convective force is no longer strong enough to extend the arms of the chain. There are no more rope-and-pulley formations. There is no "chain" at all over any part of the polymer, but only a single coil attempting to move beyond the post. We see in figure 3.5 images of a 757 Kuhn step chain at $Pe_{Kuhn} = 0.001$. The strand never forms a rope-and-pulley. Instead it eventually translates below the post as a coil.

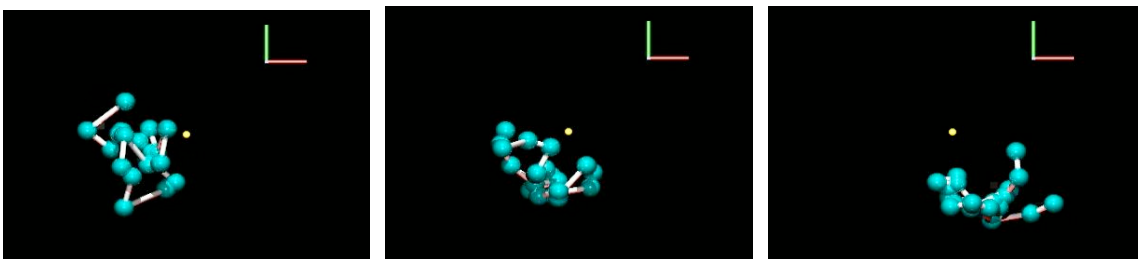

FIGURE 3.5 Images from simulations of polymers escaping from entanglements with a post, where the post is shown by a dot. This shows a 757-Kuhn-step chain under low flow ($Pe_{Kuhn} = 0.001$). The chain remains in its coiled conformation (common for Region 1 and Region 2). The "camera" is farther back because this is a long chain.

We believe that in R2 when the polymer coil collides with the post it can no longer deform and be dragged around the post. Instead, the collision will merely block the motion of the coil. The chain can move past the post only if it first diffuses a distance on the order of the radius of gyration away from the plane that passes through the post and is parallel to the flow so that the chain can clear the post without a significant collision with it. Patel and Shaqfeh[10] studied the relationship between the offset from this plane passing through the post (the so-called "y offset") and the resulting delay. Their simulation data show a gradual decrease in delay with increasing offset, but also show that the delay penalty is reduced by a factor of two or so when the offset is only about half the radius of gyration. This large drop in delay for an offset of only $R_g/2$ is reasonable, since any offset greater than $R_g/2$ will often result in weak interactions with the post and many "grazing incidences" that do not significantly slow down the coil. Also, the coil may deform somewhat in Region 2 (although not enough to form a "rope

and pulley"), and this will enable it to squeeze past the post even if it has not diffused a full radius of gyration out of the (y = 0) plane of incidence with the post. Finally, when there is an offset, in the time it takes for the coil to translate to a position that it forms a distinct entanglement contact with the post, it may diffuse farther away and completely clear the post with no delay. Hence, for simplicity, we will here approximate the results of Patel and Shaqfeh by a sharp cut-off at ½ R_g and assume that the chain cannot pass by the post until it diffuses laterally a distance ½ R_g, and when it has done so, it is free to translate beyond the post without further delay.

We use this simple picture to develop the following scaling argument and plot our data on a universal curve to show evidence of the correctness of this picture. We make two changes in the scaling of the axis from our original figure 3.1 to introduce the diffusion idea. The first change takes account of the assumption that it is the diffusion of the chain as a whole that controls the delay. We therefore use a Peclet number based on the diffusivity of the whole chain, which is given by $D = k_B T/\zeta_{total}$, and change the x-axis of figure 3.1 from Pe_{Kuhn} to Pe_{chain} where

$$Pe_{chain} = \frac{V\zeta_{tot} R_g}{k_B T} = Pe_{Kuhn}\left[\frac{\zeta_{tot} R_g}{\zeta_{Kuhn} b_K}\right] = Pe_{Kuhn}\left[\frac{N_K^{3/2}}{\sqrt{6}}\right] \tag{3.11}$$

This changes the characteristic length used in the definition of the Peclet number from the Kuhn step to the radius of gyration and the drag coefficient from that for a single Kuhn step to one for the entire chain ($\zeta_{tot} = N_K\ \zeta_{Kuhn}$).

The original measure of average delay, $\langle \Delta \bar{x} \rangle / N_K$, is a dimensionless length. Since in R2 we believe that the delay is controlled by the time it takes for the whole chain to diffuse laterally by ½ R_g, we consider two measures of time:

$$time = \frac{\langle \Delta x \rangle}{V} \tag{3.12}$$

$$time_{diff} = \frac{\left(1/2 R_g\right)^2}{D} = \frac{R_g{}^2}{4D} \tag{3.13}$$

Equation 3.12 is the average translation distance penalty divided by the fluid velocity. This is a measure of the time spent during the interaction. Equation 3.13 is a measure of the time required to diffuse a distance ½ R_g sideways from the post. A ratio of these two times is our dimensionless time.

$$\frac{time}{time_{diff}} = \frac{\langle \Delta x \rangle}{V} \frac{4D}{R_g{}^2} = \frac{\langle \Delta x \rangle}{V} \frac{4\, k_B T}{\zeta_{tot}} \frac{6}{N_K\, b_K{}^2} = \left(\frac{\langle \Delta \bar{x} \rangle}{N_K} \right) \left(\frac{24}{Pe_{Kuhn}\, N_K} \right) = z \tag{3.14}$$

Thus, the original measure of dimensionless distance, $\langle \Delta \bar{x} \rangle / N_K$, can be scaled with the inverse of Pe_{Kuhn} (a dimensionless velocity) and the ratio $24/N_K$ to give an appropriate measure of dimensionless delay time.

We plot in figure 3.6 our results for all chain lengths with this dimensionless time as the y-axis. We see that all of the data in R2 collapse onto the same curve. We note moreover that there is a plateau in the curve when the dimensionless time has a value of unity. The data for the 25 Kuhn chain deviate from the universal behavior at higher Pe_{chain} – this is because data for this chain length reach the R3/R4 regions at higher Pe_{chain} where the diffusion is no longer the key factor. We take this universal agreement among all chain lengths as strong evidence that our diffusive scaling is correct for R2.

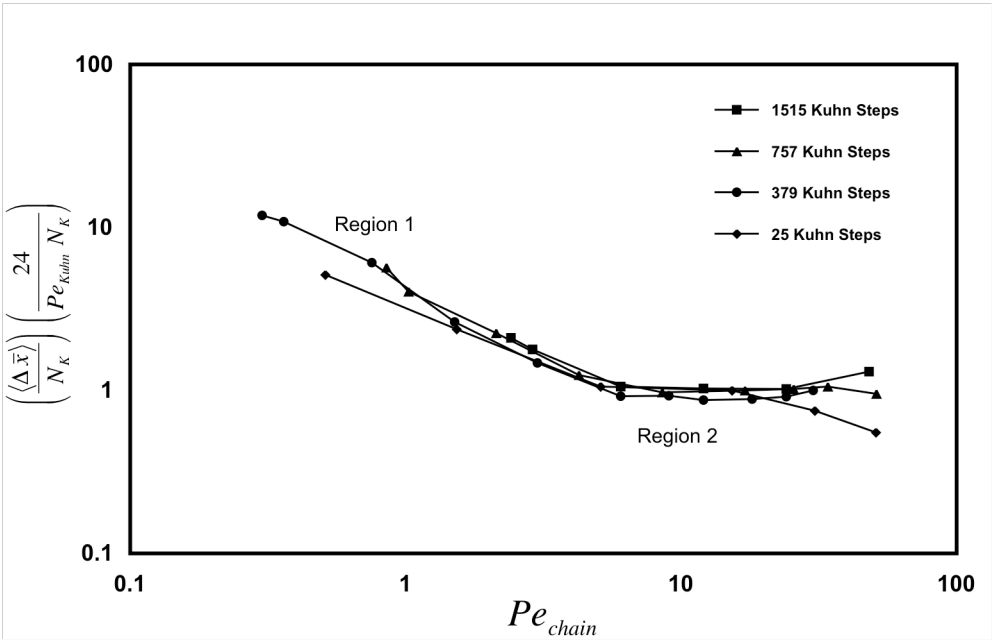

FIGURE 3.6 The data from figure 3.1 are plotted with rescaled x- and y-axes. Note that the results for all four lengths fall on a universal curve. Also note that the Region 2 plateau occurs at 1.0. This scaling is based on the diffusion-dominated physics in Region 1 and Region 2.

We further plot in figure 3.7 our delay distribution data from the longer 379 Kuhn step chain but using dimensionless time to determine the bins. We see from figure 3.1 that R2 for this chain length begins around $Pe_{Kuhn} = 0.001$ and we see on figure 3.7 that there is a clear distinction in the behavior of the data for Pe_{Kuhn} above and below this value of 0.001. The R2 results all peak at the same value of the delay time and all reach roughly the same peak probability. The data collapse onto a single curve for data in R2 – data for $Pe_{Kuhn} \geq 0.003$. An effect exactly like this is also seen for the 757-Kuhn-step and 1515-Kuhn-step chains (although the critical Pe_{Kuhn} varies for different chain lengths).

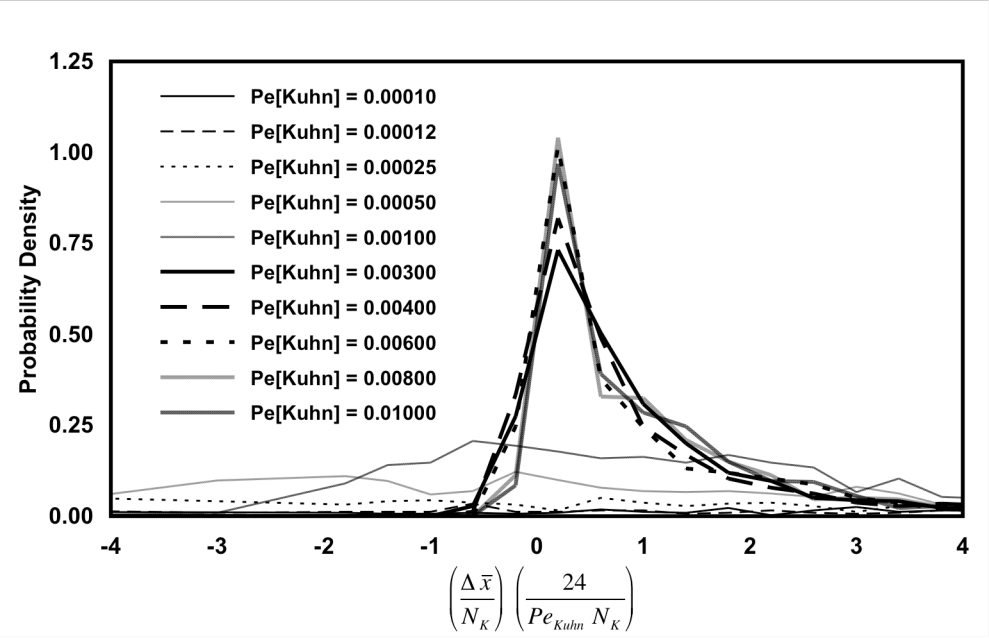

FIGURE 3.7 Rescaled probability distribution of $\left(\frac{\Delta \bar{x}}{N_K}\right)\left(\frac{24}{Pe_{Kuhn}\, N_K}\right)$ for various Pe_{Kuhn} for the 379-Kuhn-step chain simulations. Notice that the rescaled curves for $Pe_{Kuhn} > 0.001$ are nearly identical.

We show in figure 3.8a the results for all three chain lengths and for all Pe_{Kuhn} that are in R2. Note again that the x-axis is a measure of the dimensionless time. There are five data sets from R2 for the 379 Kuhn step chain, four data sets from R2 for the 757 Kuhn step chain, and three data sets from R2 for the 1515 Kuhn step chain. We are pleased to see that all these results collapse (roughly) into a single curve for all Pe_{Kuhn} and N_K within R2. This is additional strong evidence that our diffusion scaling is sound. The individual peaks occur at the same dimensionless time but their magnitude varies somewhat, in a manner that does not seem to correlate with either Pe_{Kuhn} or N_K.

We note our picture for the dynamics in R2, in which we assume that the delay is entirely due to the time required for the coil to diffuse laterally a distance of $R_g/2$, is equivalent to a classical "first-passage-time" problem. In this problem, one seeks to determine the time required for a random diffuser to reach a fixed distance from its starting point. There is a distribution of times, and this distribution is a function of the diffusivity of the object and the distance it is required to travel. We actually have a "double-sided first-passage-time" problem because the coil can pass the post on either side. Nagar and Pradhan present this distribution of double-sided first-passage times for a one dimensionally diffusing object[16]

$$P(t,L) = \sum_{n=1}^{\infty} (-1)^{n+1} \frac{D(2n-1)\pi}{L^2} \exp\left[-\frac{(2n-1)^2 \pi^2 D}{4L^2} t\right] \tag{3.15}$$

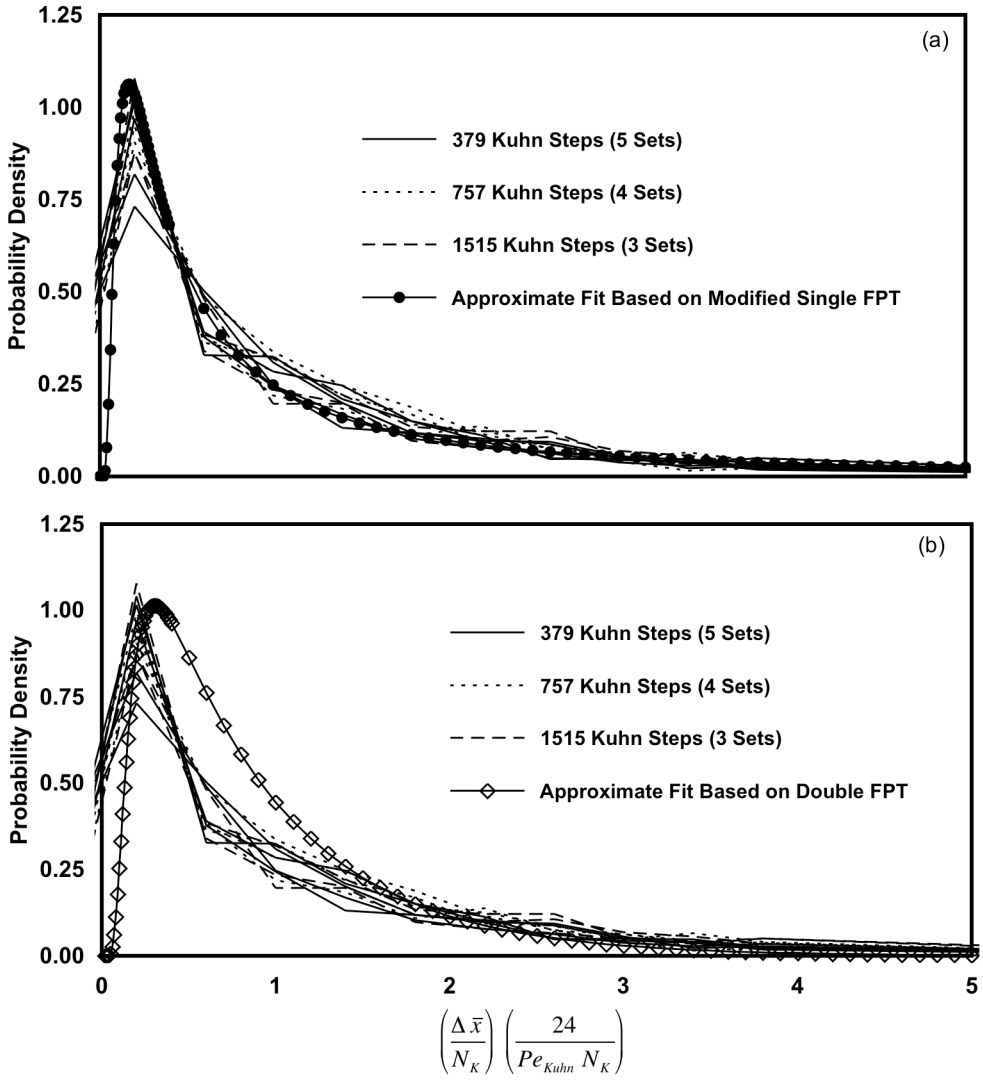

FIGURE 3.8 Rescaled probability distribution of $\left(\frac{\Delta \bar{x}}{N_K}\right)\left(\frac{24}{Pe_{Kuhn}\, N_K}\right)$ restricted to Pe_{Kuhn} values in Region 2 for the chains with 379 Kuhn steps, 757 Kuhn steps, and 1515 Kuhn steps. These are independent of Pe_{Kuhn} or N_K. In part (a), the solid circles are a phenomenological fit to the simulation data based on a modified single-sided first-passage-time, equation 3.25 (with $\beta = 0.02$). In part (b), the open diamonds show the prediction based on the double-sided first-passage-time, equation 3.22 (with $\alpha = 1.35$).

where L is the distance that must be traveled, D is the diffusivity, and t is the required time. We recast equation 3.15 in dimensionless variables to align this formula with our nomenclature for R2. We choose $L = \alpha\left(R_g/2\right)$ as the distance the polymer coil must travel (based on our previous comment about the results from Patel and Shaqfeh) where α is a parameter that will allow us to adjust the distance to best fit our results. We therefore make the following substitutions

$$L = \alpha\frac{1}{2}R_g = \alpha\frac{1}{2}\left(\frac{N_K {b_K}^2}{6}\right)^{1/2} \tag{3.16}$$

$$D = \left(\frac{k_B T}{N_K \zeta_K}\right) \tag{3.17}$$

$$t = \frac{\Delta x}{V} \tag{3.18}$$

This transforms equation 3.15 into

$$P(t,L)\,dt = \sum_{n=1}^{\infty}(-1)^{n+1}\frac{\left[\frac{k_B T}{N_K\zeta_K}\right](2n-1)\pi}{\left(\frac{1}{4}\right)\left[\frac{N_K {b_K}^2}{6}\right]\alpha^2}\exp\left[\frac{(2n-1)^2\pi^2\left[\frac{k_B T}{N_K\zeta_K}\right]\left[\frac{\Delta x}{V}\right]}{-4\left(\frac{1}{4}\right)\left[\frac{N_K {b_K}^2}{6}\right]\alpha^2}\right]\frac{d(\Delta x)}{V} \tag{3.19}$$

Using the original definition of Pe_{Kuhn} (equation 3.1) and the expression for the dimensionless time (equation 3.14), equation 3.19 will simplify to

$$P(t,L)\,dt = \sum_{n=1}^{\infty}(-1)^{n+1}\frac{(2n-1)\pi\left(\frac{24}{Pe_K N_K}\right)}{N_K\, b_K\, \alpha^2}\exp\left[-\frac{(2n-1)^2\pi^2 z}{4\alpha^2}\right]d(\Delta x) \tag{3.20}$$

The final step is to replace the *d(Δx)* with *dz* (see equation 3.14):

$$d(\Delta x) = dz\left[\frac{Pe_K\; b_K\; N_K{}^2}{24}\right] \tag{3.21}$$

The result is

$$P(z)\,dz = \sum_{n=1}^{\infty}(-1)^{n+1}\frac{(2n-1)\pi}{\alpha^2}\exp\left[-\frac{(2n-1)^2\pi^2 z}{4\alpha^2}\right]dz \tag{3.22}$$

We plot equation 3.22 on figure 3.8b to compare the predictions of this simple double-sided first-passage-time theory with our simulation results. This approximation is successful in predicting the scaling, but it does a poor job of matching the results. We find $\alpha = 1.35$ to give the closest agreement with our data. This would imply that the actual distance the coil must diffuse (on average) out of the plane of the post is 0.675 R_g (close to the ½ R_g that we had discussed previously). The idea of a double-sided first-passage-time is a good match for the physical description but it is a crude approximation for the data. Presumably, because of fluctuations and small deformations, the chain does not always require the same offset to squeeze by the post, and even when it has enough

clearance to pass the post unobstructed, it may occasionally drift back in front of the post before passing it by.

Rather than attempt to develop a better physical model, to summarize our simulation results with a simple analytical formula, we seek a better fit for the R2 results by resorting to an empirical formula. We find that the solution to the *single-sided* first-passage-time, where the coil must reach a certain distance in, say, the positive direction, actually does a good job describing our data (and this does not require the α parameter to scale the length measure). We admit that this is an empirical method. The solution to this single-sided problem is presented by Mazo[17]

$$P(\xi,t)\,dt = \frac{\xi}{\sqrt{4\pi D t^3}} \exp\left[\frac{-\xi^2}{4Dt}\right] dt \tag{3.23}$$

where ξ is the measure of distance, D is the diffusivity, and t is the required time. We repeat the scaling procedure described above to recast equation 3.23 as a function of z.

$$P(z) = \frac{1}{\sqrt{4\pi z^3}} \exp\left[-\frac{1}{4z}\right] \tag{3.24}$$

We recognize that equation 3.24, while fitting the distribution of delay times well, has an infinite mean. (The actual mean in the simulations is set by the extreme tail of the distribution function and the infinite mean does not prevent the above distribution function from providing a good fit to the simulation data over the range of delay times

considered.) The infinite mean will be a problem later as we seek to use this approximation to determine the variance. We therefore need to make one additional small correction to equation 3.24 so that it will have a finite mean. We multiply the function by a rapidly decreasing exponential $\left(\exp\left[-\beta z\right]\right)$. We also must divide by $\left(\exp\left[-\sqrt{\beta}\right]\right)$ to normalize the probability to unity.

$$P^*(z) = \frac{1}{\sqrt{4\pi z^3}} \exp\left[-\frac{1}{4z}\right] \frac{\exp\left[-\beta z\right]}{\exp\left[-\sqrt{\beta}\right]} \tag{3.25}$$

We plot equation 3.25 on figure 3.8a to compare the predictions of this empirical function (based on the single-sided first-passage-time theory) with our simulation results. We find $\beta = 0.02$ to give the closest agreement with our data. We note that the mean value of equation 3.25 is around 3.5. We would expect, from figure 3.6, that the mean value of z in R2 would be close to unity. This discrepancy can be attributed to the arbitrary manner in which we elected to alter equation 3.24 to result in a finite mean. A mean of 3.5 is much closer to unity than a mean of infinity is. A more complicated extra term may have accomplished both tasks (getting a finite mean *and* getting a mean of unity). However, we accept equation 3.25 as a sufficient approximation for our later use.

3.3.4 Region (R1)

Region 1 (R1) is where the convective force is very weak compared to the diffusive force. This is the very-slow-flow regime. Note in figure 3.1 that for all four chain

lengths, we have data in this region, and that the data all fall along the same line (this line can be fit to a power law that scales as $Pe_{Kuhn}^{0.27}$).

As with R2, the polymer in R1 does not reach the rope-and-pulley formation because there is insufficient force to fully extend the chain. The polymer must translate beyond the post by randomly diffusing out of the plane containing the post and the flow direction and then be moved downstream of the post by convective motion.

However, in R1, it is possible for a chain to diffuse far enough laterally to be able to clear the post but is convected so slowly that it might frequently diffuse *back* into line with the post before clearing it. It might therefore need to clear the post multiple times before the coil is able to move beyond the post. We note that in figure 3.6 the transition from R2 to R1 happens at the same Pe_{chain} for all lengths of chain.

Note that some negative times appear for the R1 curves on figure 3.7. In this very low Pe_{Kuhn} regime, where diffusion dominates the motion, it is possible for a coil to have moved downstream *faster* than it would have if it were carried by the flow alone. To explore this, we ran the two sets of simulations, $N_K = 379 \;/\; Pe_{Kuhn} = 0.003$ (this is in R2) and $N_K = 379 \;/\; Pe_{Kuhn} = 0.001$ (this is in R1), both with and without the post in the field. Figure 3.9a shows the comparison in R2. Note that the run without the post yields a distribution of delay distances centered and symmetric about zero, as expected, and the average delay time is zero. The run with the post in R2 has a peak to the positive side of zero and has a lengthy tail on the positive side, with relatively few molecules having a

negative delay, indicating that while lateral diffusion determines the time required for the chain to clear the post (as discussed earlier), longitudinal diffusion (i.e., in the flow direction) is less important than convection, in determining the distribution of delay distances, especially in the tail region. We note that the relative importance of longitudinal diffusion compared to convection is influenced by the distance (about seven Kuhn step lengths) that the chain must travel down field to reach the "finish line" where the simulation stops and the time to reach this "finish line" is recorded. If we had put the "finish line" farther down field, there would have been more time for both convection and diffusion to operate, but the importance of longitudinal diffusion, *relative* to convection would have been diminished, and the fraction of chains with a negative "delay" time would have been smaller. The average delay time, which is the time to reach the "finish line" minus the time required for a chain purely convected in the absence of the post, for this run was greater than zero – indicating that the post had an influence on the chain.

Figure 3.9b shows the comparison in R1. Note that in this case there is only a small difference between the runs *with* and *without* the post. The average delay time for the run *without* the post is zero while it is slightly greater than zero when the post is present. In R1 the delay time is dominated by longitudinal diffusion and the presence of the post merely perturbs that diffusion.

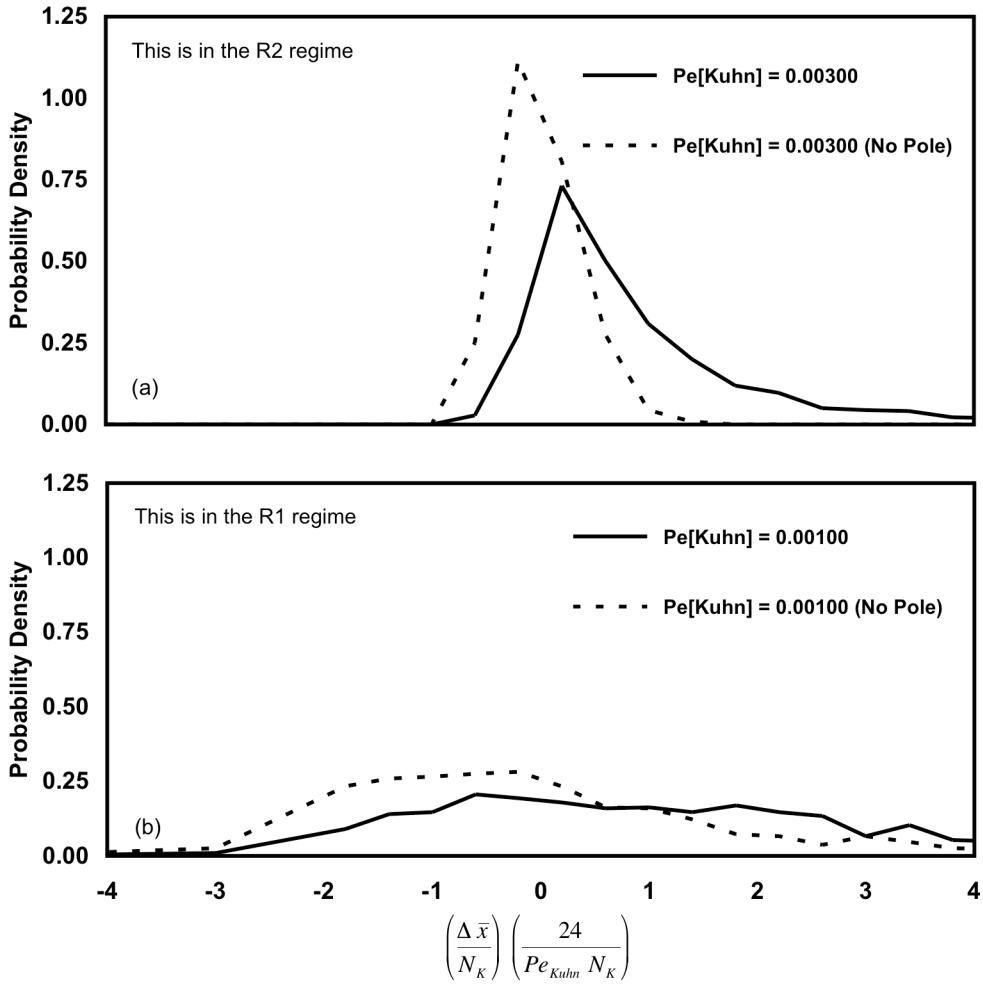

FIGURE 3.9 Rescaled probability distribution of $\left(\frac{\Delta \bar{x}}{N_K}\right)\left(\frac{24}{Pe_{Kuhn}\, N_K}\right)$ *with* and *without* the post for Regions 1 and 2. (a) Region 2: $N_K = 379$ and $Pe_{Kuhn} = 0.003$. (b) Region 1: $N_K = 379$ and $Pe_{Kuhn} = 0.001$.

The asymmetry of the distribution even without the post is due to the manner in which we run the simulations. All simulations begin with the random coil placed a small distance upstream of the post. This is done such that the most downstream bead of the coil is

initially located one-tenth of a radius of gyration upstream of the post. The average location of the center of mass of the coil in this set-up will vary based on chain length – a larger chain will have its center begin farther away from the post even though chains of all lengths have their most downstream bead in roughly the same place. The center of mass for the 379-Kuhn-step chain begins (on average) 7.5 Kuhn steps upstream of the post while the center of mass for the 1515-Kuhn-step chain begins (on average) 16 Kuhn steps upstream of the post. All simulations end when the bead that is closest to the post (the leftmost bead in a left to right flow) is located seven-and-a-half Kuhn steps downstream beyond the post. Again, the location of the center of mass of the chain when this occurs will vary with the number of Kuhn steps in the chain. A longer chain will have its center of mass farther downstream than a shorter chain, when the simulation ends. The location of the center of mass will also vary as a function of Pe_{Kuhn} – chains under more aggressive flow conditions will be more stretched in the direction of the flow and their center of mass will be farther downstream.

We find that this is a relatively short distance (7.5 Kuhn steps beyond the post) to the "finish line." We must compare the difference in the starting location of the center of mass and the finishing location of the center of mass. This is the distance that the chain has traveled in a finite amount of time. The time required for a chain to transverse this distance minus the time required to transverse the same distance in the absence of diffusion has a bound on the negative side. This leads to a negative bound for z which varies as a function of chain length and Pe_{Kuhn}. (Recall that z is a function of Pe_{Kuhn}, N_K, and, $\langle \Delta \bar{x} \rangle$). For example, z cannot be more negative than -70.4 for $N_K = 379$ and

$Pe_{Kuhn} = 0.0001$, even if the chain were instantaneously to jump from its starting position to the finish line. There is no upper bound on the positive delay time; hence, the distribution of delay times is asymmetric about zero, even in the absence of the post.

Since R1 is controlled by the subtle perturbation to the distribution of delay times that the post introduces, and the distance to the finish line likely influences significantly the behavior in R1, predicting even semi-quantitatively the behavior in this regime would be rather difficult. In addition, since chain motion is so slow, this regime is probably also of limited importance to electrophoretic separation. Hence we content ourselves here with the qualitative description of the behavior in R1 that we have just given.

3.3.5 Mean And Variance

We have developed in this work formulas that predict the probability distributions in R4/R3 (equation 3.7) and R2 (equation 3.25). Note that R4 is defined by equation 3.7 when *b = 0*. We now evaluate the mean and variance in each of these regions. We first must re-write equation 3.25 in terms of $\Delta \bar{x}/N_K$.

$$P^*\left(\frac{\Delta \bar{x}}{N_K}\right) = \frac{\left(\frac{24}{Pe_K N_K}\right)}{\sqrt{4\pi\left(\frac{24}{Pe_K N_K}\right)^3\left(\frac{\Delta \bar{x}}{N_K}\right)^3}} \exp\left[\frac{-\left(\frac{Pe_K N_K}{24}\right)}{4\left(\frac{\Delta \bar{x}}{N_K}\right)}\right] \frac{\exp\left[-\beta\left(\frac{24}{Pe_K N_K}\right)\left(\frac{\Delta \bar{x}}{N_K}\right)\right]}{\exp\left[-\sqrt{\beta}\right]} \qquad (3.26)$$

Using equation 3.7 and equation 3.26, we find

	$MEAN(\mu)$	$VARAIANCE(\sigma^2)$	$\frac{\sigma^2}{\mu^2}$
R4	$\frac{1}{2}$	$\frac{1}{4}$	1
R3	$\frac{1}{2}-b$	$\frac{1}{4}-b^2$	$\frac{0.25-b^2}{1-2b+b^2}$
R2	$\frac{1}{2\left(\frac{24}{Pe_K N_K}\right)\beta^{1/2}}$	$\frac{1}{4\left(\frac{24}{Pe_K N_K}\right)^2\beta^{3/2}}$	$\frac{1}{\sqrt{\beta}}$

TABLE 3.1 The mean and variance for each of the three highest regions. This is for a single chain interacting with a single post.

Recall that $b = f(Pe_K, N_K)$ and that $\beta = 0.02$. We plot in figure 3.10 the dimensionless ratio σ^2/μ^2 for chains with various Pe_K and N_K. We note that all chains reach the same value $(\sigma^2/\mu^2) = 1$ at high Pe_K and all chains have the same value $(\sigma^2/\mu^2) = 7.07$ at low Pe_K. It is only in R3 where σ^2/μ^2 depends on Pe_K for chains of different lengths.

The value of Pe_K at which the ratio σ^2/μ^2 for Region 2 intersects the value of σ^2/μ^2 = 7.07 for Region 3 is marked on figure 3.1 with the large asterisk mark. This depends on N_K. Note that this mark is a good measure of where the mean reduced delay $\langle \Delta \bar{x} \rangle / N_K$ for each chain shows a transition between R3 and R2 behavior. The agreement between the crossover as measured by the intersection of the values of σ^2/μ^2 and as measured by

the crossover in the value of $\langle \Delta \bar{x} \rangle / N_K$ is better with the three longer chains – but we have commented earlier that the R3 approximation is less likely to be successful for chains with a small number of Kuhn steps.

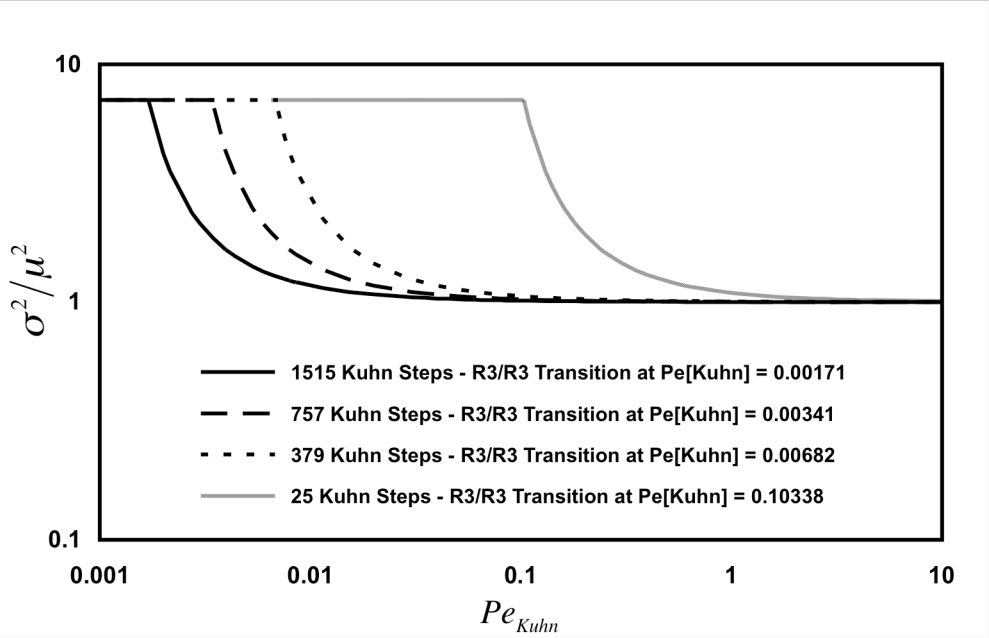

FIGURE 3.10 A plot of σ^2/μ^2 for four different length chains. σ^2/μ^2 = 1 for all chains in the high-field regime, R4. σ^2/μ^2 = 7.07 for all chains in the low-field regime, R2. σ^2/μ^2 is a function of Pe_{Kuhn} and N_K in the intermediate-field regime R3. The values of Pe_{Kuhn} for the transitions between R2 and R3 are shown with large asterisks on figure 3.1.

Our simulations have dealt only with the interaction of a single chain with a single post. However, we can apply our findings qualitatively to the more useful case of a chain interacting with a sparse array of posts, by first considering a row of posts arrayed

perpendicular to the migration distance (with a spacing which we will discuss momentarily) and then considering n columns of these rows of posts in succession, allowing the chain to interact successively with one row after the next. This will be a simplified but useful extrapolation from the work presented in this paper to the case of a "sparse" array of posts. This can be combined with some of the work of Dorfman[12] to develop a full model for an array of sparse posts.

We have been assuming in each simulation that each chain is aligned with the post. We can imagine a situation where there is a row of posts with a well-defined spacing between each post. A chain may approach this row and, depending on the spacing, either have an entanglement interaction with a post or pass through between two posts unaffected. For simplicity, we shall take a "step function" approach to the interactions, and assume that the collision is either effectively a "head on" collision of the type we have analyzed here, or a "clean miss." That is, the off-center collisions are treated as either close enough to being head on that they can treated as such, or are lumped into those that experienced a "clean miss." We will define f to be the probability of an effective head-on collision and 1-f the probability of an effective clean miss. From the discussion above, f will be approximately given as the ratio between R_g and the distance separating two posts in the same row. The percentage of "clean misses" will affect both σ^2 and μ for the average interaction of the chain with the first row. The "total" mean, incorporating the misses, is easily calculated as $\mu_T = f\mu$.

It is more complicated to determine the average total variance for the interaction with the row of posts. Consider the probability of delay to be a combination of two terms – the first term being the probability P that we discussed earlier and the second term being a delta function at zero (representing a miss). The contribution from each term is weighted by *f*.

$$P_T\left(\frac{\Delta\bar{x}}{N_K}\right) = f\,P\left(\frac{\Delta\bar{x}}{N_K}\right) + (1-f)\,\delta\left(\frac{\Delta\bar{x}}{N_K}\right) \tag{3.27}$$

The variance of equation 3.27

$$\sigma_T{}^2 = \int_0^\infty \left(\frac{\Delta\bar{x}}{N_K} - f\mu\right)^2 f\,P\left(\frac{\Delta\bar{x}}{N_K}\right) d\left(\frac{\Delta\bar{x}}{N_K}\right) + \int_0^\infty \left(\frac{\Delta\bar{x}}{N_K} - f\mu\right)^2 (1-f)\,\delta\left(\frac{\Delta\bar{x}}{N_K}\right) d\left(\frac{\Delta\bar{x}}{N_K}\right) \tag{3.28}$$

is found after some mathematics to be

$$\sigma_T{}^2 = f\sigma^2 + 2\mu^2 f(1-f) - \mu^2 f\left(1-f^2\right) + \mu^2 f^2(1-f) \tag{3.29}$$

σ^2 and μ have already been determined for each region. Equation 3.29 provides a simple expression for the adjusted variance as a function of σ^2, μ, and *f* for a row of equally spaced posts with any post density. The ratio $\sigma_T{}^2/\mu_T{}^2$ is then determined as

$$\frac{\sigma_T{}^2}{\mu_T{}^2} = \frac{1}{f}\frac{\sigma^2}{\mu^2} + \frac{1}{f}2(1-f) - \frac{1}{f}\left(1-f^2\right) + (1-f) \tag{3.30}$$

Note that, for $f = 1.0$, this returns the original σ^2/μ^2.

We now consider an array of *n* columns of these post rows. Both the variance and the mean will scale with *n*. If the rows of posts are spaced widely enough apart that a DNA molecule can completely relax after any encounter it experiences in the first row of posts before it encounters a post in the second array, we can take each encounter to be independent of the others. Then, according to the central limit theory, for large n, a set of DNA molecules of given length passing through the array of posts will emerge distributed as a Gaussian with mean delay $n\mu_T$ and standard deviation $\sqrt{n}\sigma_T$. The relative width of the peak, which is the ratio of the standard deviation to the mean, scales, inversely with the square root of *n*.

$$\text{relative peak width} = \frac{1}{\sqrt{n}} \frac{\sigma_T}{\mu_T} \tag{3.31}$$

Since the above formula allows one to determine the bandwidths and resolution of different bands of migrating DNA, it could be used to design an array that can electrophoretically separate DNA strands by size. It is important to note that this is for a dilute DNA solution in a sparse array of posts. The posts must be sufficiently sparse that the chain is able to re-form the random coils between interactions. The simulation method we have used here could also be used to determine the interactions of a DNA molecule with multiple, more densely arrayed, posts, where the interactions of the molecule with one post are coupled to the interactions with other posts. Such coupled

interactions could take place either because the spacing in a single row is tight enough for the chain to interact simultaneously with more than one post, or because the column spacing is small enough that the molecule does not recover completely from one interaction before it has another. One can imagine combining the results of such simulations with the formulas we have derived above by using "interaction coefficients" to adjust the dilute-post formulas for the effects of more densely arrayed posts, thus producing empirically useful formulas for designing such arrays for DNA separations. However, such additional work is beyond the scope of this study. A theory that converts single entanglement encounters into expressions predicting separation parameters has been put forward by Dorfman, who, however, did not consider the low-field cases (R1 through R3) that we have explored here.

3.4 SUMMARY

We have used our previously developed bead-spring Brownian dynamics model to simulate the interactions between a polymer chain and a thin obstacle. We studied electrophoretically translating DNA strands entangling with an immovable post, sampling a wide range of chain lengths ($25 \le N_K \le 1500$) and spanning four orders of magnitude in field strength ($10^{-4} \le Pe_{Kuhn} \le 10^{0}$). We found that the delay in chain migration distance created by the entanglement is greater at higher fields, and that there are four distinct regimes that describe these entanglements, two of which (R3 and R4) are dominated by convection, and two (R1 and R2) by diffusion. We discussed the physics that govern the four regions and for all but the first region (lowest field strength) we presented analytic

approximations for the distribution of delay distances, including the mean and standard deviation of the delay.

The high field strength region (R4) is characterized by rope-and-pulley interactions in which there is sufficient convective force for the polymer always to reach a fully extended configuration. Previous work[6] has shown that all chains (regardless of length) reach a limit of $\langle \Delta \bar{x} \rangle / N_K = 0.5$ in this region. In a region with a less dominant convective force (R3) the chain is not able to fully extend its arms on other side of the obstacle. Hence, the polymer does not form the rope-and-pulley configuration; instead it forms more of a chain-and-clump configuration in which the size (the number of monomers) of the clump is inversely related to the field strength. This results in shorter-lived interactions than were present in R4. While limitations of computer time prevented us from generating simulation data for R3 for the longer chains, we were able to developed a model to predict the behavior in R3 including the variation of $\langle \Delta \bar{x} \rangle / N_K$ with N_K and Pe_{Kuhn}, and this model agreed well with the simulation data that we were able to obtain.

In the two slower regimes (R2 and R1), the convective force is not able to alter significantly the shape of the polymer, and the chain retains a coil-like shape as it diffuses laterally and eventually passes the post largely without deforming. We argue that the controlling effect in R2 is the time required for the coil to diffuse a distance ½ R_g out of the plane of the post. We rescaled our data based on this argument and found universal behavior of all chain lengths in this regime. We also developed an approximation for this

region based on the solution to the first-passage time problem. While lateral diffusion controls the delay distance in Region 2, with negligible effect of longitudinal diffusion, in the slowest region (R1), convection is so slow that the distribution of delay times is dominated by longitudinal diffusion that is perturbed subtly by interactions with the post. Prediction even semi-quantitatively the behavior in this regime would be rather difficult. We also note that R1 features a peculiar fractional power law relationship $\langle \Delta \bar{x} \rangle / N_K \propto Pe_{Kuhn}^{0.27}$.

Our results are unique in addressing a comprehensive range of electrophoretic strengths and chain lengths and in providing accurate analytical expressions for the distribution of delay distances induced by a single post. We find the mean and variance of the probability distribution for each of the three fastest regimes, and use these along with the central limit theorem to generalize our results from a single chain interacting with a single post to a dilute solution of chains interacting with a sparse array of posts. Our methods can readily be extended to consider the effect of non-sparse arrays, with potential applications in the field of size dependant separations.

REFERENCES

[1] Barron, A.E.; Soane, D.S.; Blanch, H.W. *Journal of Chromatography A* **1993**, *652*, 3.

[2] Doyle, P.S.; Bibette, J.; Bancaud, A.; Viovy, J.L. *Science* **2002** *295*, 2237.

[3] Volkmuth, W.D.; Austin, R.H. *Nature* 1992, *358*, 600.

[4] Volkmuth, W.D.; Duke, T.; Wu, M.C.; Austin, R.H. *Physical Review Letters* **1994**, *72*, 2117.

[5] Randall, G.C.; Doyle, P.S. *Physical Review Letters* **2004**, *93*, 058102.

[6] Randall, G.C.; Doyle, P.S. *Macromolecules* **2006**, *39*, 7734.

[7] Starkweather, M.E.; Muthukumar, M.; Hoagland, D.A. *Macromolecules* **1998**, *31*, 5495.

[8] Nixon, G.I.; Slater, G.W. *Physics Review E* **1994**, *50*, 5033.

[9] Saville, P.M.; Sevick, E.M. *Macromolecules* **1999**, *32*, 892.

[10] Patel, P.D.; Shaqfeh, E.S.G. *Journal of Chemical Physics* **2003**, *118*, 2941.

[11] Padding, J.T.; Briels, W.J. *Journal of Chemical Physics* **2002**, *117*, 925.

[12] Dorfman, K.D. *Physics Review E* **2006**, *73*, 061922.

[13] Holleran, S.P.; Larson, R.G. *Rheological Acta* **2007**, in press.

[14] Li, L.; Larson, R.G. *Macromolecules* **2000,** *33*, 1411.

[15] Hsieh, C.; Jain, S.; Larson, R.G. *Journal of Chemical Physics* **2006**, *124,* 044911.

[16] Nagar, A.; Pradhan, P. *Physica A* **2003**, *320*, 141.

[17] Mazo, R.M. *Brownian Motion: Fluctuations, Dynamics, and Applications*; Clarendon Press Oxford, 2002.

CHAPTER 4

SUMMARY AND FUTURE WORK

4.1 SUMMARY OF RESEARCH

This purpose of this research was to develop a method to model the interactions between an electrophoretically translating polymer chain and a stationary obstacle, and to use that method to analyze the types of entanglements that occur at various field strengths. One application of this research is in the area of size-dependant separation of DNA strands.

We began with traditional bead-spring Brownian dynamics simulations and we added a repulsive force that can act between two springs or between a spring and an obstacle. We are able to determine the distance separating each spring and the post, and the repulsive force is a function inversely related to that distance. It is an achievement of this work that we are able to use bead-spring BD because this allows us to simulate very long DNA strands ($N_K > 1500$) – strands which would be too computationally expensive to be modeled with established bead-rod BD.

Our work is unique in that it permits the springs to pass through the post during a time step (the spring can be "broken") but we accordingly correct for this in the subsequent

timestep. This quality allows our method to use a much larger time step (because we are not concerned with nearly infinitely high repulsive forces in the region very close to the post) and we are able to quickly simulate larger chains.

Our method was tested for robustness and convergence with respect to the strength and range of the repulsive force, the choice of time step, and the number of beads used to model polymers of a particular length.

We measured an ensemble-averaged delay distance to quantify the effect of the polymer-post interaction. This is a measure of distance showing the difference between a chain's location in a simulation containing the obstacle and in a simulation without the obstacle for the same field strength. We are able to replicate, using our bead-spring technique, the results of a previously published simulation[1] that had used bead-rod BD as its method.

We have the ability to explore four orders of magnitude in field strength ($10^{-4} \le Pe_{Kuhn} \le 10^{0}$) and this proved very fortunate as we discovered interesting and unexpected behavior in the very low field regimes. We modeled polymers over a wide range of lengths ($25 \le N_K \le 1500$). We used two types off spring laws – the worm-like-chain was used for the longer springs ($N_K > 350$) and FENE-Fraenkel[2] was used for the 25 Kuhn step chain (because it is a better model for short springs).

We found that there are four different types of entanglement events that occur, each occurring over a region determined by the ratio of convective force to diffusive force

(Pe_{Kuhn}). We described the mechanisms for the entanglement and escape in each of the regions. "Rope-and-pulley" interactions are common in the two highest field regions. There is sufficient convection to extend the arms of the chain (the chain is fully extended in the highest region). Our findings agree with Randall and Doyle[3] in that all chains reach an upper limit of $\langle \Delta \bar{x} \rangle / N_K = 0.5$ in the highest field region. We proposed that the chain is unable to become fully extended at lower Pe_{Kuhn} and that the result of this is a chain-and-clump orientation in which the ends of each arm are a collection of coiled monomers. The size of this clump has an influence on the average time of the interaction – more monomers in the clump will reduce the average entanglement time.

The two slower regions are characterized by the chain's inability to leave its original coiled formation. Diffusion is dominant in this case. We believe that the polymer can get beyond the post by diffusing out of the plane and then being convected downstream. We developed a scaling based on this diffusive argument – and we found our results for the two slowest regions fall on a universal curve independent of chain length.

We developed analytical expressions to predict $\langle \Delta \bar{x} \rangle / N_K$ as a function of Pe_{Kuhn} in each of the three highest field regions. We used our prediction from Region 3 to complete some of the missing data from our plot of $\langle \Delta \bar{x} \rangle / N_K$ vs. Pe_{Kuhn} and we found that our prediction does an excellent job of bridging the gap between Region 2 and Region 4. We used these analytical expressions to calculate the mean and variance in each region in the case of a single polymer chain entangled with a single stationary post. We extrapolated our findings to become applicable to line of evenly spaced posts. We then discussed a

manner to convert a line of posts into an array of posts. This returned our project to its original goal of developing a method for size-dependant separation of DNA strands.

4.2 POTENTIAL FUTURE WORK

There are a number of problems that can benefit from the work of this dissertation. I will initially discuss two cases that can be reasonable next steps based on the bead-spring BD method that we have developed.

It is possible to consider the self-entanglement of a single polymer chain under various flow conditions (particularly under a shearing flow). Traditional bead-spring BD simulations do not enforce repulsions between the springs, and this allows the polymer chain to continuously pass through itself as it sample configurations. Our method can be used to apply a repulsive force between springs in the same polymer (rather than between each spring and a post). A test of the success of this idea would be to compare the average radius of gyration of a chain simulated using traditional bead-spring BD to that of a chain simulated using our new bead-spring BD method. It would also be valuable to compare those results to the radius of gyration found by experimentation.

A second use of our bead-spring BD method could be to study the dynamics of a semi-dilute solution of polymer chains. There are two significant adjustments to be made in this situation. The number of repulsive force calculations in each time would be much greater because it would be necessary to monitor each spring-spring interaction (both

along the same chain and from one chain to another). A creative algorithm or a clever use of the nearest neighbors principle may reduce the intensity of this process. Additionally, it is different from the work we have presented here in that the obstacle (one of the other polymers in the dilute solution, in this case) will translate in the direction of the flow as the entanglement is happening. The two molecules will translate together with an effective mass equal their sum, they will move together while simultaneously undergoing the "rope-and-pulley" entanglement action. For some applications, filling a channel with a dilute solution of neutral polymers may be more advisable than etching a channel with stationary posts, and these simulations will describe this situation.

One final avenue for future work is something we discussed at the end of chapter 3. The work we have presented here is focused on a single polymer chain interacting with a single stationary obstacle. We did some theoretical work to predict the effects that an array of posts would have on the mean and variance of the ensemble-averaged delay distance. This is applicable in designing a channel of posts suited to separate polymer chains of varying lengths. Dorfman[4] has also previously done some theoretical work in this field. More concrete work can be done in this area using the simulation method that we have developed. The simulation method we have used here could also be used to determine the interactions of a DNA molecule with multiple, more densely arrayed posts, where the interactions of the molecule with one post are coupled to the interactions with other posts. Such coupled interactions could take place either because the spacing in a single row is tight enough for the chain to interact simultaneously with more than one

post, or because the column spacing is small enough that the molecule does not recover completely from one interaction before it has another. Our work can be used to study the effects of multiple posts – to determine the ideal spacing and post density – and to optimize the design of the post array.

REFERENCES

[1] Patel, P.D.; Shaqfeh, E.S.G. *Journal of Chemical Physics* **2003**, *118*, 2941.

[2] Hsieh, C.; Jain, S.; Larson, R.G. *Journal of Chemical Physics* **2006**, *124,* 044911.

[3] Randall, G.C.; Doyle, P.S. *Macromolecules* **2006**, *39*, 7734.

[4] Dorfman, K.D. *Physics Review E* **2006**, *73*, 061922.